Accepted Manuscript

Pyrrolidine nucleoside bisphosphonates as antituberculosis agents targeting hypoxanthine-guanine phosphoribosyltransferase

Wai Soon Eng, Dominik Rejman, Radek Pohl, Nicholas P. West, Kyra Woods, Lieve M.J. Naesens, Dianne T. Keough, Luke W. Guddat

PII: S0223-5234(18)30811-0

DOI: 10.1016/j.ejmech.2018.09.039

Reference: EJMECH 10750

To appear in: *European Journal of Medicinal Chemistry*

Received Date: 19 April 2018

Revised Date: 10 August 2018

Accepted Date: 14 September 2018

Please cite this article as: W.S. Eng, D. Rejman, R. Pohl, N.P. West, K. Woods, L.M.J. Naesens, D.T. Keough, L.W. Guddat, Pyrrolidine nucleoside bisphosphonates as antituberculosis agents targeting hypoxanthine-guanine phosphoribosyltransferase, *European Journal of Medicinal Chemistry* (2018), doi: https://doi.org/10.1016/j.ejmech.2018.09.039.

Biological Data for **6** (below) with *Mycobacterium tuberculosis*

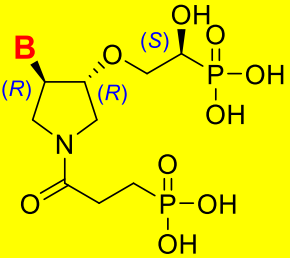

B = guanine

K_i = 60 nM for *Mt* HGPRT; IC_{50} = 14 uM virulent *Mt* ;

IC_{50} = 29 uM latent *Mt* IC_{50} = 85 uM macrophage model

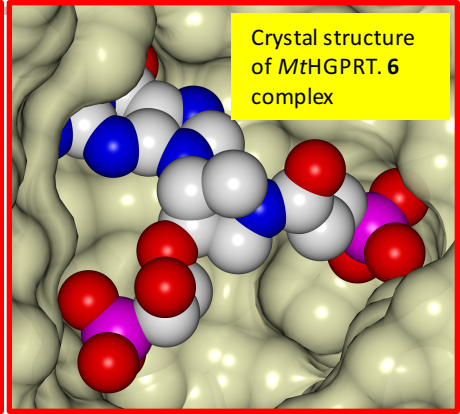

Pyrrolidine Nucleoside Bisphosphonates as Antituberculosis Agents Targeting Hypoxanthine-Guanine Phosphoribosyltransferase

Wai Soon Eng[†], Dominik Rejman*[‡], Radek Pohl[‡], Nicholas P. West[†], Kyra Woods[†], Lieve M. J. Naesens[§], Dianne T. Keough[†] and Luke W. Guddat*[,†]

[†]*School of Chemistry and Molecular Biosciences, The University of Queensland, Brisbane, 4072 QLD, Australia*

[‡]*Institute of Organic Chemistry and Biochemistry, Academy of Sciences of the Czech Republic, v.v.i. Flemingovo nam. 2, CZ-166 10 Prague 6, Czech Republic*

[§]*Rega Institute for Medical Research, KU Leuven – University of Leuven, Herestraat 49, B-3000 Leuven, Belgium*

Address for correspondence: Luke Guddat: luke.guddat@uq.edu.au School of Chemistry and Molecular Biosciences, The University of Queensland, Brisbane, 4072 QLD, Australia

Dominik Rejman: dominik.rejman@uochb.cas.cz Institute of Organic Chemistry and Biochemistry, Academy of Sciences of the Czech Republic, v.v.i. Flemingovo nam. 2, CZ-166 10 Prague 6, Czech Republic

Abbreviations: TB, Tuberculosis; *Mt*, Mycobacterium tuberculosis; HGPRT, hypoxanthine-guanine phosphoribosyltransferase; MDR, multidrug resistant; XDR, extensively drug-resistant; $PP_{i,}$ pyrophosphate; *P*Rib-*PP*, 5-phospho-α-D-ribosyl-1-pyrophosphate; ANP, acyclic nucleoside phosphonate; PNP, pyrrolidine nucleoside phosphonates; PNBP, pyrrolidine nucleoside bisphosphonates; AIP, acyclic immucillin phosphonate

Keywords: *Mycobacterium tuberculosis*; therapeutic drug leads; X-ray crystal structures; hypoxanthine-guanine phosphoribosyltransferase; pyrrolidine nucleoside phosphonates; pyrrolidine nucleoside bisphosphonates; phosphoramidate prodrugs

Abstract

Therapeutic treatment of tuberculosis (TB) is becoming increasingly problematic due to the emergence of drug resistant *Mycobacterium tuberculosis* (*Mt*). Thus, new targets for anti-TB drug discovery need to be identified to combat and eradicate this disease. One such target is hypoxanthine-guanine phosphoribosyltransferase (HGPRT) which synthesises the 6-oxopurine nucleoside monophosphates essential for DNA/RNA production. [3*R*,4*R*]-4-Hypoxanthin-9-yl-3-((*S*)-2-hydroxy-2-phosphonoethyl)oxy-1-*N*-(phosphonopropionyl)pyrrolidine and [3*R*,4*R*]-4-guanin-9-yl-3-((*S*)-2-hydroxy-2-phosphonoethyl)oxy-1-*N*-(phosphonopropionyl)pyrrolidine (compound **6**) are the most potent inhibitors of *Mt*HGPRT yet discovered having K_i values of 60 nM. The crystal structure of the *Mt*HGPRT.**6** complex was obtained and compared with that of human HGPRT in complex with the same inhibitor. These structures provide explanations for the 60-fold difference in the inhibition constants between these two enzymes and a foundation for the design of next generation inhibitors. In addition, crystal structures of *Mt*HGPRT in complex with two pyrrolidine nucleoside phosphosphonate inhibitors plus pyrophosphate provide insights into the final stage of the catalytic reaction. As the first step in ascertaining if such compounds have the potential to be developed as anti-TB therapeutics, the tetra-(ethyl L-phenylalanine) tetraamide prodrug of **6** was tested in cell based assays. This compound arrested the growth of virulent *Mt* not only in its replicating phase (IC_{50} of 14 μM) but also in its latent phase (IC_{50} of 29 μM). Furthermore, it arrested the growth of *Mt* in infected macrophages (MIC_{50} of 85 μM) and has a low cytotoxicity in mammalian cells (CC_{50} of 132 ± 20 μM). These inhibitors are therefore viewed as forerunners of new anti-TB chemotherapeutics.

1. Introduction

Mycobacterium tuberculosis (*Mt*) is the predominant etiological agent for human tuberculosis (TB).[1] TB remains a global public health threat, with 10 million cases of active disease per annum resulting in 1.8 million deaths.[2] Current treatment for TB is a standard six-month regimen of rifampicin and isoniazid, supplemented with pyrazinamide and ethambutol in the first two months.[3] However, the emergence of multidrug-resistant *Mt* (MDR-TB)[4] and extensively drug-resistant *Mt* (XDR-TB)[5] has limited the capacity to eradicate this disease. A major obstacle in eradication is the development of drugs that efficiently target both the replicating and non-replicating/dormant stages of *Mt*.[6] For example, when in dormancy, *Mt* is insensitive to the frontline drug, isoniazid.[7] Thus, there is an urgent need for new cost-effective TB therapeutics directed against not only the replicating stage of this pathogen but also its dormant (latent/persistent) stage. Crucially, apart from bedaquiline, which has associated toxicity concerns[8] and is currently the subject of clinical investigation,[9-10] it has been more than 50 years since a new therapeutically viable anti-TB drug was commercially introduced onto the market.[11]

Evidence that hypoxanthine-guanine phosphoribosyltransferase is a target for the development of anti-TB therapeutics comes from two sources. The first is a random transposon mutagenesis study which showed that the expression of this enzyme is essential for the survival of *Mt*.[12] The second is a recent study which showed that prodrugs of inhibitors of *Mt* hypoxanthine-guanine phosphoribosyltransferase (*Mt*HGPRT) activity arrested the growth of a virulent strain of *Mt* in cell culture.[13] Thus, began the search for the design of new and more potent inhibitors which could also posses anti-TB activity.

*Mt*HGPRT catalyses the formation of the nucleoside monophosphates, IMP or GMP, and pyrophosphate (PP_i). The substrates are 5-phospho-α-D-ribosyl-1-pyrophosphate (*P*Rib-*PP*) and hypoxanthine (Hx) or guanine (G); xanthine is not a substrate.[13-14] For catalysis to occur, a divalent

metal ion, usually magnesium, is required (**Fig. 1**). Literature reports suggest that the mechanism of action of *Mt*HGPRT is ordered and sequential,[15] similar to that of human HGPRT.[16] However, the kinetic parameters for the two enzymes are very different. *P*Rib-*PP*, for example, has a much higher K_m for *Mt*HGPRT than for human HGPRT with values of 465 μM with guanine as the base and 1443 μM with hypoxanthine as the base[13-14] compared with 60 μM and 30 μM, respectively, for human HGPRT.[16-17] The values for the purine bases, however, differ by only two-fold with the K_m for guanine and hypoxanthine being 4.4 and 8.3 μM for *Mt*HGPRT[13, 17] while, for human HGPRT, these values are 1.9 and 3.4 μM,[17] respectively. The k_{cat} values for these two enzymes in the forward reaction are also widely different. *Mt*HGPRT has a k_{cat} values of 0.6 s^{-1} (guanine as base) and 0.5 s^{-1} (hypoxanthine as base)[13] while, for human HGPRT, the k_{cat} values are 10-fold higher, 8.2 s^{-1} (guanine) and 5.2 s^{-1} (hypoxanthine).[17] The tetrameric structure of both enzymes also differ in the arrangement of their subunits. Thus, in the quaternary structure of the human enzyme, the large mobile loop which moves to cover the active site during catalysis is located on the outside of the structure where, in its open position, it is exposed to solvent. In contrast, this loop is buried at the interface of the dimer pairs in *Mt*HGPRT.[13] Whether this structural arrangement has an effect on the kinetic constants is, however, unknown at present.

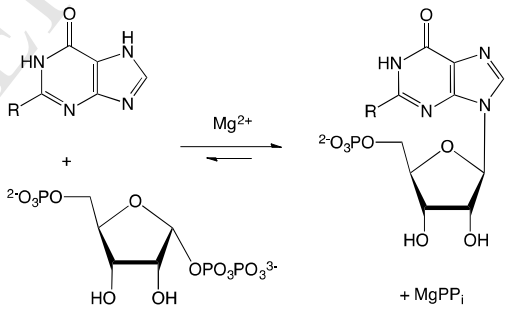

Fig. 1. The reaction catalysed by *Mt*HGPRT. R = -H (hypoxanthine); $-NH_2$ (guanine). The other naturally-occurring purine base, xanthine (R = -OH), is not a substrate.[13-14]

The only reported inhibitors of *Mt*HGPRT to date are the acyclic nucleoside phosphonates (ANPs).[13] Their structure consists of a phosphonate moiety connected to a nucleobase via an acyclic linker. The advantage of using these compounds as a template for therapeutics is the presence of the carbon phosphorus bond within the phosphonate moiety which makes them enzymatically and chemically stable within the cell.[18] The genesis for these potential anti-TB drugs is based on structure of the successful antiviral agent tenofovir that was developed by Antonin Holý and colleagues.[18] Prodrugs of the ANPs arrest the growth of *Pf* in cell culture[19-21] highlighting the possibility that selective design could lead to the development of chemotherapeutics against *Mt* where the activity of this enzyme also appears to be essential for the survival and reproduction of this organism.

Pyrrolidine nucleoside monophosphonates (PNPs) inhibit the two 6-oxopurine PRTases from *Escherichia coli,* XGPRT and HPRT,[22] *Plasmodium falciparum* HGXPRT[19], *Plasmodium vivax* HGPRT [19] and human HGPRT.[19, 22] In these compounds, a purine base is attached to a phosphonate moiety via a pyrrolidine ring in the linker which connects the two functional groups. The five membered pyrrolidine ring is connected to the N^9 atom of the purine base (**Fig. 1**), as is the ribose moiety of the products of the catalytic reaction, GMP and IMP. The basic structure of this class of inhibitor is shown in **Fig. 2** indicating their structural diversity and how and where chemical modifications can be made to increase their potency for the 6-oxopurine phosphoribosyltransferases from different organisms. For example, different chemical attachments can be made at the carbon (R^1) and/or the nitrogen (R^2) position of the pyrrolidine ring (**Fig**. **2**).

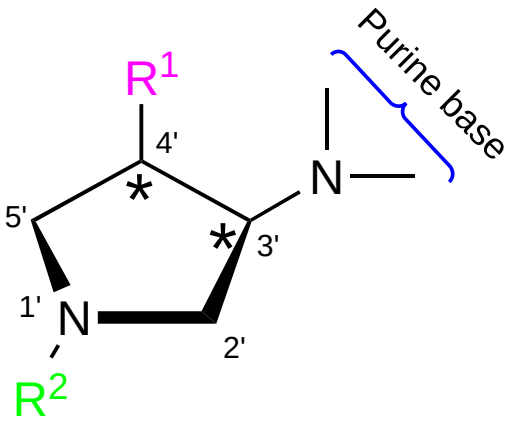

Fig. 2. The chemical structure of the phosphonates which contain a pyrrolidine ring in the linker. The pyrrolidine group can be attached to any purine base at the 9-position in the imidazole ring. R^1 and R^2 denote where different chemical moities can be attached to the pyrrolidine ring. In the two pyrrolidine nucleoside monophosphonates (PNPs) described here, a phosphonate group is attached at the R^1 position and, in the pyrrolidine nucleoside bisphosphonates (PNBPs), a second phosphonate group is attached at R^2. The (*) shows the stereocenters.

In this report, eight compounds containing a pyrrolidine group in the acyclic linker were trialled as inhibitors of *Mt*HGPRT (**Fig. 3**). Two of these belong to the purine nucleoside monophosphonate (PNP) class of compounds while six belong to the pyrrolidine nucleoside bisphosphonates (PNBPs) class. The first class contains a single phosphonate group while the second contains two phosphonate groups. X-ray crystal structures of the two PNPs, ([3*R*,4*R*]-(4-(hypoxanthin-9-yl)pyrrolidin-3-yl)-oxymethanephosphonic and [3*R*,4*R*]-(4-(guanin-9-yl)pyrrolidin-3-yl)oxymethanephosphonic acid were obtained in complex *Mt*HGPRT in the presence of pyrophosphate. The X-ray structure of one of the PNBPs, ([3*R*,4*R*]-4-guanin-9-yl-3-((*S*)-2-hydroxy-2-phosphonoethyl)oxy-1-*N*-(phosphonopropionyl)pyrrolidine) (**6**) in complex with *Mt*HGPRT was also obtained. This structure was then compared with that of the human counterpart in complex with the same inhibitor to explain the 60-fold difference in the K_i values and to provide the necessary tools to

improve their design aimed at increasing potency for *Mt*HGPRT. In order to determine if such coumpounds have the potential for further development as anti-TB agents, a tetra-(ethyl L-phenylalanine) tetraamide prodrug of **6** was tested against TB in cell culture. These studies were done under aerobic (reflecting the replicating stage of its life cycle) and hypoxic (reflecting its dormant stage) conditions. The effect of this prodrug on the growth of the bacillus in infected macrophages and its cytotoxicity in mammalian cells *in vivo* were also determined.

2. Results and Discussion

2.1. Chemistry

Figures 3 and **4** give the chemical structures of the eight compounds examined in this study. The synthesis and chemical analysis of **1**, **2**, **5**, **6** and **8** have been reported previously.[19, 22] The methodology for the synthesis of **3**, **4**, and **7** is presented in **Scheme 1**; the synthesis of the new compounds **3**, **4**, and **7** follows the same experimental procedures described in a previous report.[23]

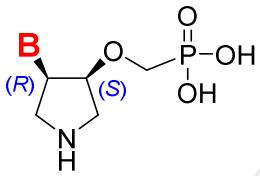

1 (**B** = Hx); **2** (**B** = guanine)

Fig. 3. The pyrrolidine nucleoside phosphonates (PNPs) where the purine base (B) is either hypoxanthine or guanine. **1**: [3*S*,4*R*]-(4-(Hypoxanthin-9-yl)pyrrolidin-3-yl)-oxymethanephosphonic acid**; 2**: [3*S*,4*R*]-(4-(Guanin-9-yl)pyrrolidin-3-yl)oxymethanephosphonic acid.

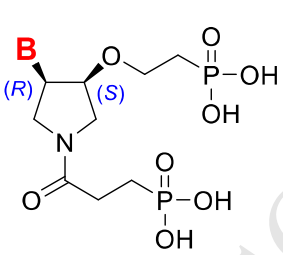

3 (**B** = Hx); **4** (**B** = guanine)

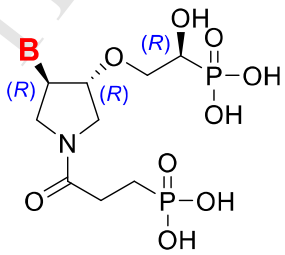

5 (**B** = Hx); **6** (**B** = guanine)

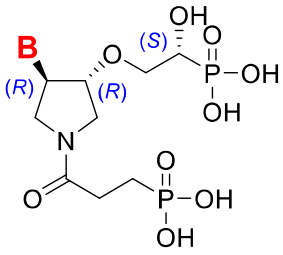

7 (**B** = Hx); **8** (**B** = guanine)

Fig. 4. The pyrrolidine nucleoside bisphosphonates (PNBPs) where the purine base (B) is either hypoxanthine or guanine: [3*R*,4*S*]-4-hypoxanthin-9-yl-3-(2-phosphonoethyl)oxy-1-*N*-(phosphonopropionyl)pyrrolidine (**3**), [3*R*,4*S*]-4-guanin-9-yl-3-(2-phosphonoethyl)oxy-1-*N*-(phosphonopropionyl)pyrrolidine (**4**), [3*R*,4*R*]-4-hypoxanthin-9-yl-3-((*S*)-2-hydroxy-2-phosphonoethyl)oxy-1-*N*-(phosphonopropionyl)pyrrolidine (**5**), [3*R*,4*R*]-4-guanin-9-yl-3-((*S*)-2-hydroxy-2-phosphonoethyl)oxy-1-*N*-(phosphonopropionyl)pyrrolidine (**6**), [3*R*,4*R*]-4-hypoxanthin-9-

yl-3-((*R*)-2-hydroxy-2-phosphonoethyl)oxy-1-*N*-(phosphonopropionyl)pyrrolidine (**7**), and [3*R*,4*R*]-4-guanin-9-yl-3-((*R*)-2-hydroxy-2-phosphonoethyl)oxy-1-*N*-(phosphonopropionyl)pyrrolidine (**8**).

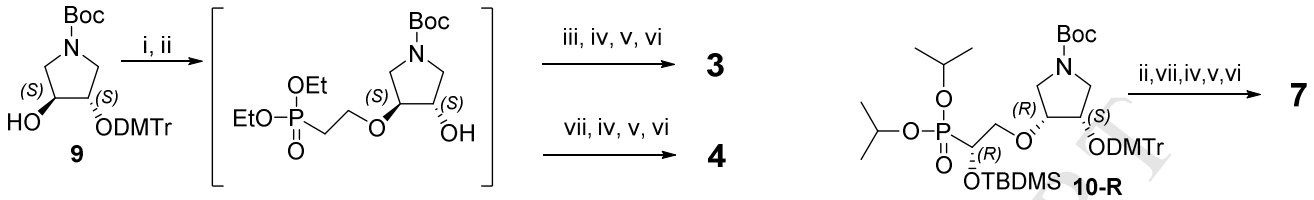

i. Diethyl vinylphosphonate, t-BuOH, KOH, Cs_2CO_3; ii. 2%TFA/$CHCl_3$; iii.6-chloropurine, Ph_3P, DIAD, THF; iv. 1.5M HCl/H_2O-EtOH 1:1, 75 °C; v. diisopropyl 3-phosphonopropionic acid, EDC, DMF, 80 °C; vi. Me_3SiBr, MeCN; vii. 2-amino-6-chloropurine, Ph_3P, DIAD.

Scheme 1. Synthetic scheme for compounds **3**, **4**, and **7**.

2.2. Inhibition of MtHGPRT activity

The K_i values of the eight compounds for *Mt*HGPRT are given in **Table 1**. These values are compared with those for human HGPRT.

Table 1. The K_i values for the pyrrolidine inhibitors of *Mt*HGPRT and human HGPRT

Code	K_i (μM)		K_i ratio	Code	K_i (μM)		K_i ratio
	Mt	Human	*Mt*/human		*Mt*	Human	*Mt*/human
	Base is hypoxanthine				*Base is guanine*		
1	88±4	327±70	0.3	**2**	8±0.4	29±10	0.3
1	3 ± 4[a]	ND[b]	-	**2**	0.74±0.1[a]	ND[b]	ND
3	0.42±0.04	0.6±0.06	0.7	**4**	0.04±0.01	0.03±0.01	1.3
5	0.06±0.004	0.001±0.0007[c]	60	**6**[c]	0.06±0.01	0.003±0.001[c]	20
7	0.20±0.02	0.008±0.002[c]	25	**8**[c]	0.13±0.01	0.008±0.003[c]	16

[a]Addition of 400 μM pyrophosphate to the assay. [b]ND = not determined. [c] see reference 19

These eight compounds exhibit a wide range of selectivity in their K_i values for *Mt*HGPRT and human HGPRT, 0.3 to 60 fold (**Table 1**). Compounds **1** and **2** have much lower K_i values for

*Mt*HGPRT compared with human HGPRT (ratio of 0.3), compounds **3** and **4** do not discriminate (ratios of 0.7 and 1.3) while, for compounds **5** and **6** as well as compounds **7** and **8**, the selectivity is reversed with the K_i values being lower for human enzyme compared with *Mt*HGPRT (ratios of 16 to 60) (**Table 1**). Together with the dissimilarities in the kinetic constants for the naturally-occurring substrates, this data suggests differences in the structure of their active sites.

Table 1 shows that the chemical nature of the phophonate moiety effects the K_i values. Furthermore, it also appears to effect how the purine bases bind. For example, compounds **1**, **2**, **3** and **4**, have lower K_i values for both enzymes when guanine is the base but, for compounds **5**, **6**, **7** and **8**, the K_i values are similar, irrespective of whether the base is guanine or hypoxanthine (**Table 1**).

PP_i, at a concentration of 400 μM in the assay, does not inhibit *Mt*HGPRT activity (*cf*. 5.7 nmoles min^{-1} in its absence with 6.6 nmoles min^{-1} in its presence). However, when PP_i is added to the assay together with either of the PNPs (**1** or **2**), the K_i value for the PNP decreases by 30- and 11- fold (**Table 1**), suggesting that PP_i binds in the active site together with **1** or **2**, thus effecting the kinetic constants. The decrease in the K_i values could occur by PP_i, re-positioning the PNP to a more optimal location. Schramm and his colleagues have demonstrated that the tight binding complexes of the transition state analogs, immucillin-G 5′-phosphate or immucillin-H 5′-phosphate with human HGPRT and *Pf*HGXPRT, respectively, are only obtained in the presence of $MgPP_i$ as all three sites need to be occupied.[24-26] The K_i values are significantly lower for *Mt*HGPRT with compounds **3**, **4,** **5**, **6**, **7** and **8** compared with **1** and **2** (220-1466 fold, hypoxanthine as base; 61-200 fold, guanine as base). These ratios fall to 7.5-50 and 5-20 when PP_i is added to the assay with compounds **1** and **2**. Thus, a reasonable proposition is that the primary reason for this large decrease is due to the attachment of a second covalently linked phosphonate group to compounds **3**, **4,** **5**, **6**, **7** and **8**. This second phosphonate group would then be expected to occupy the PP_i binding site. The K_i values for

*Mt*HGPRT of **4**, **5** and **6** are the lowest yet determined for this enzyme (**Table 1**) as the best previous value is 1 μM.[13]

Crystal structures of *Mt*HGPRT in complex with **1**, **2** or **6** were, therefore, obtained to explain how these inhibitors bind in the active site so as to be able to modify their design to produce compounds with even lower K_i values. The structures of the *Mt*HGPRT.**6** complex and the human HGPRT.**6** complex were compared to discover if differences exist in their mode of binding in their active sites.

2.3. Crystal structures of MtHGPRT in complex with two PNPs and a BPNP.

2.3.1. Overall structure.

Crystal structures of *Mt*HGPRT in complex with **1** plus PP_i, **2** plus PP_i and **6** were determined at 2.44 Å, 2.55 Å and 2.91 Å resolution, respectively. The data collection and refinement statistics are presented in **Table S1**. All three complexes crystallized as a tetramer in the asymmetric unit and there is strong electron density for each of the inhibitors in all four active sites of the tetramer (**Fig. 5**). For compound **2**, PP_i was added directly to the enzyme, together with the inhibitor, five minutes before adding this mixture to the well solution. For **1**, however, PP_i was not added to the enzyme though electron density corresponding to this structure was found in the active site. The presence of PP_i in this structure appears to have arisen due to the magnesium catalysed hydrolysis of *P*Rib-*PP*.[27] *Mt*HGPRT is stored in 0.1 M Tris-HCl, 0.012 M $MgCl_2$, pH 7.4 containing 200 μM *P*Rib-*PP*, -80 ^oC, under which conditions it is stable for >2 years.[13]

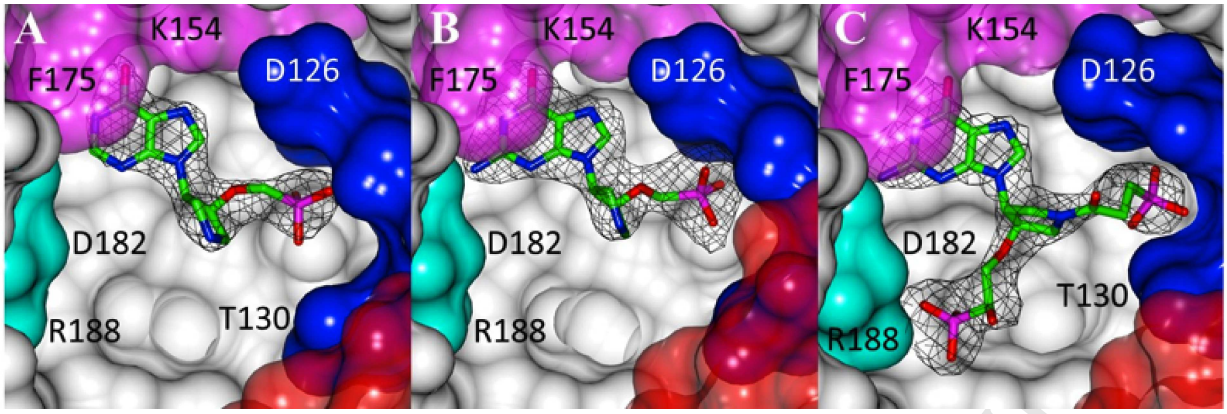

Fig. 5. F_o-F_c omit electron density map and the structure of the three inhibitors overlayed onto the Connolly surface of *Mt*HGPRT. (**A**) **1,** (**B**) **2,** (**C**) **6.** For simplification, the electron density for PP_i in the active site has not been included in **Figs**. **5A** and **B**.

The RMSD values upon superimposition of Cα atoms in these three complexes are presented in **Table S2**. These data show that there are only minimal differences in the overall fold (0.22 to 0.36 Å) when the three structures are compared. When dimer halves of *Mt*HGPRT are superimposed (lower diagonal), the RMSD values are only marginally smaller and range from 0.22 to 0.37 Å. This suggests that the presence of inhibitors in the active site does not influence the association of the four subunits. Thus, the differences in affinity of the three pyrrolidine inhibitors are not due to major structural changes in the enzyme.

2.3.2. The active site of MtHGPRT

Fig. 6 identifies key areas of *Mt*HGPRT proposed to be involved in binding of key functional groups. These areas are based on the amino acid sequence and deductions from known crystal structures.[13] **Figs. 7**, **8** and **9** show the specific interactions that the atoms of each of the three inhibitors form with active site residues.

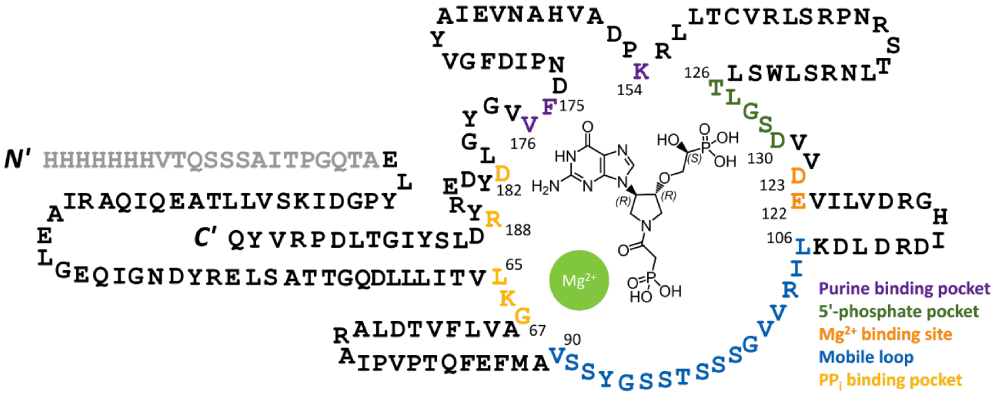

Fig. 6. Amino acid sequence of *Mt*HGPRT. The chemical structure of **6** is inserted in this figure to show where functional groups would be expected to bind. The residues contained in the large mobile loop proposed to close over the active site during catalysis (residues V90-L106) are shown in blue.

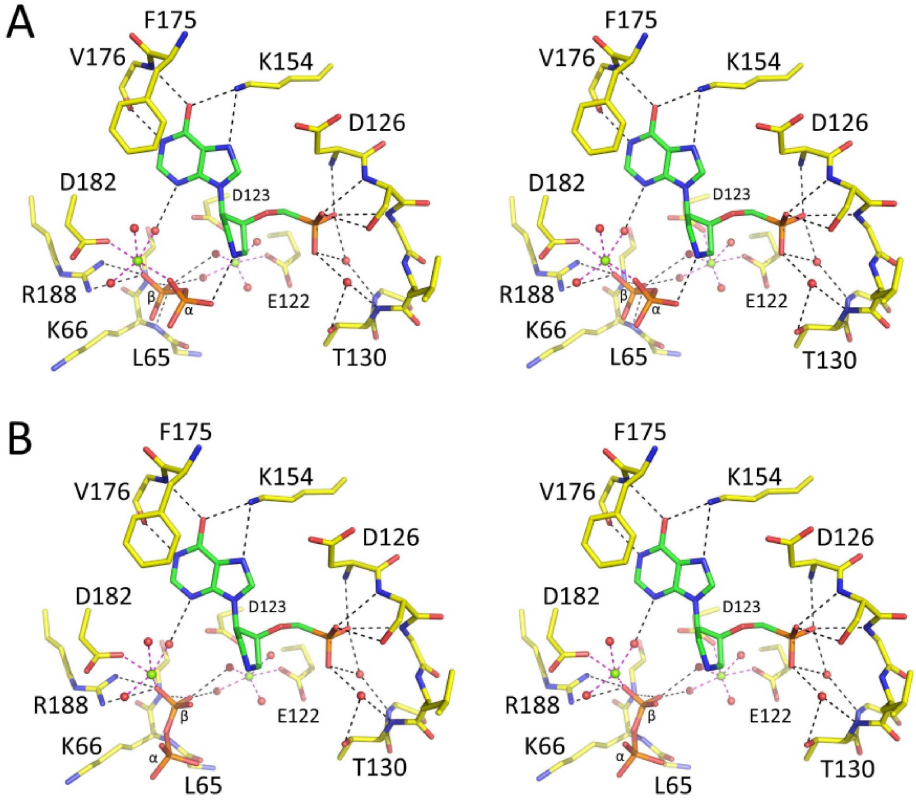

Fig. 7. Stereoview of the active site of the *Mt*HGPRT.**1**.PP_i complex. Each subunit contains two molecules of pyrophosphate. (**A**) shows the location of one of the PP_i molecules and (**B**) shows the location of the second. Solid spheres represent Mg^{2+} ions (green) and waters (red).

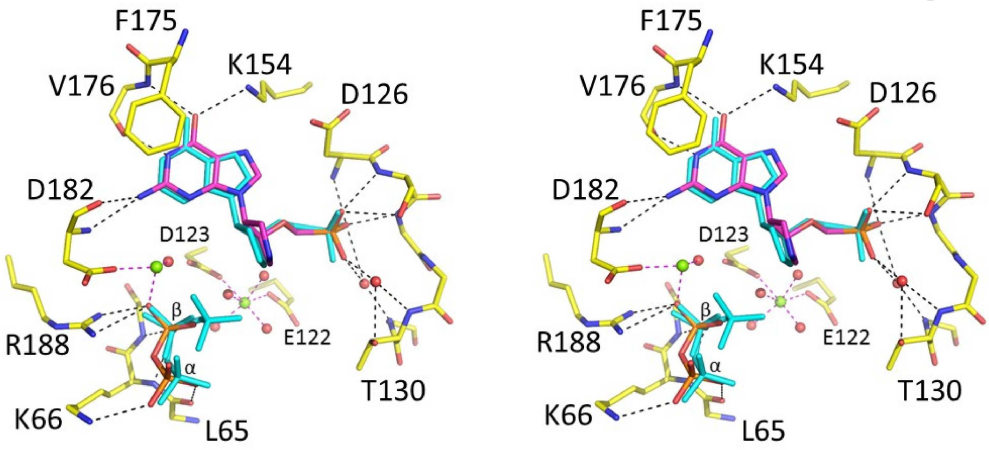

Fig. 8. Stereoview of the active site of the *Mt*HGPRT.**2**.PP_i complex (subunit A). Compound **2** has the carbon atoms in magenta and PP_i is drawn in red and orange. There is only one PP_i in each of the four active sites but it has two different orientations. Subunits A and B have one orientation while subunits C and D have the second. Solid spheres represent the two Mg^{2+} ions (green) and waters (red) in the *Mt*HGPRT.**2**.PP_i complex. The structure of **1** and PP_i (cyan) when bound to *Mt*HGPRT is superimposed for comparison.

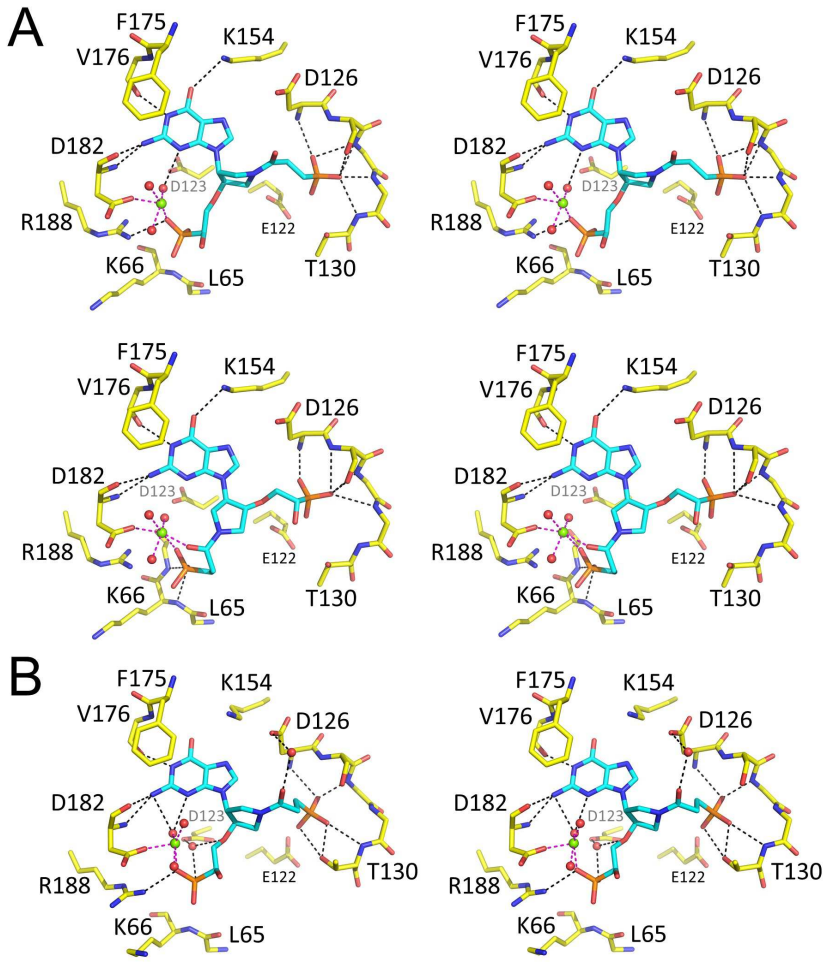

Fig. 9. Stereo view of the active site of the *Mt*HGPRT.**6** complex. (**A**) Subunit A (*top*: occupancy of **6** is 60%; *bottom*: occupancy of **6** is 40%). (**B**) Subunit B. The inhibitor has the same orientation in subunits B, C and D and this is the same as the top panel in (**A**). The single Mg^{2+} ion and water molecules are shown as green and red spheres, respectively.

Figs. 10A and **10B** compare the location of PP_i in the *Mt*HGPRT.**1** or **2** complexes with that of PP_i in human HGPRT.**ImmGP.**PP_i complex.[25] **Fig. 10C** compares the location of the phosphonate group pointing down into the predicted PP_i binding site in the *Mt*HGPRT.**6** with that of the phosphonate group in the human HGPRT.**6** complex[19] and the human HGPRT.**ImmGP.**PP_i complex.[25]

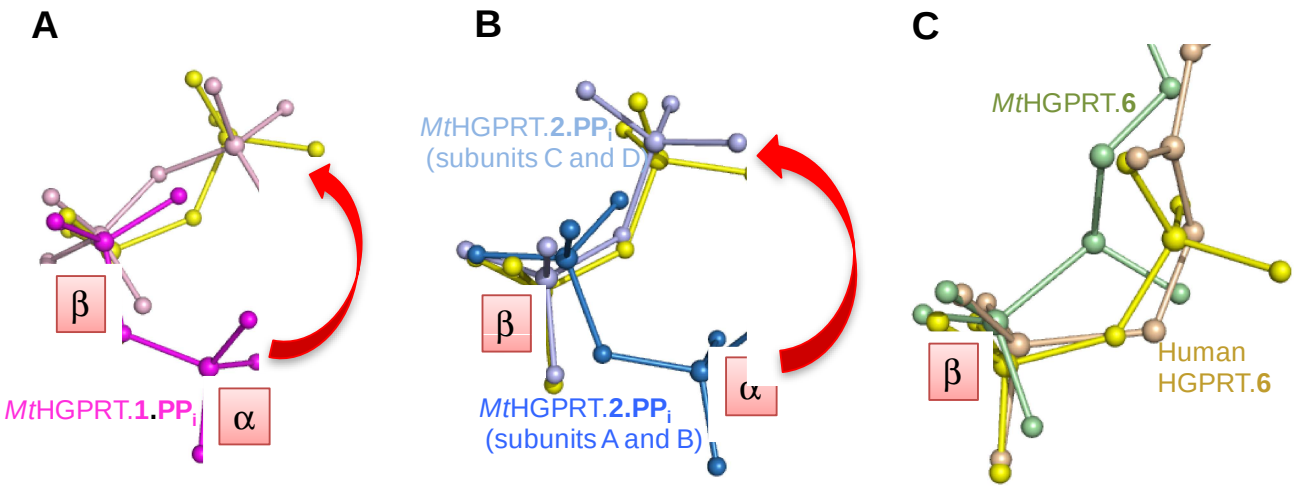

Fig. 10. The pyrophosphate binding site in *Mt*HGPRT. The crystal structures are superimposed on that of the HGPRT.**ImmGP**.**PP$_i$** complex (yellow). (**A**) The location of the two PP$_i$ molecules present in all four subunits in the *Mt*HGPRT.**1**.PP$_i$ complex. (**B**) The location of the single PP$_i$ molecule in subunits A and B (dark blue) or C and D (pale blue) in the *Mt*HGPRT.**2**.PP$_i$ complex (**C**) Superimposition of *Mt*HGPRT.**6** (green) with human HGPRT.**6** (wheat).[19] α and β correspond to the positions of the phosphorus atoms shown in **Figs**. **7** and **8**. The red arrows in **A** and **B** show the rotation of the phosphorus atom (α).

Superimposition of the three *Mt*HGPRT structural complexes reveal the differences in the location of these three inhibitors in the active site. These lie in four areas: (i) the location and orientation of the pyrrolidine ring; (ii) the position of the phosphonate group located in the 5′-phosphate binding pocket; (iii) the location and the number of magnesium ions; and (iv) the position of the purine base (**Fig. 11**).

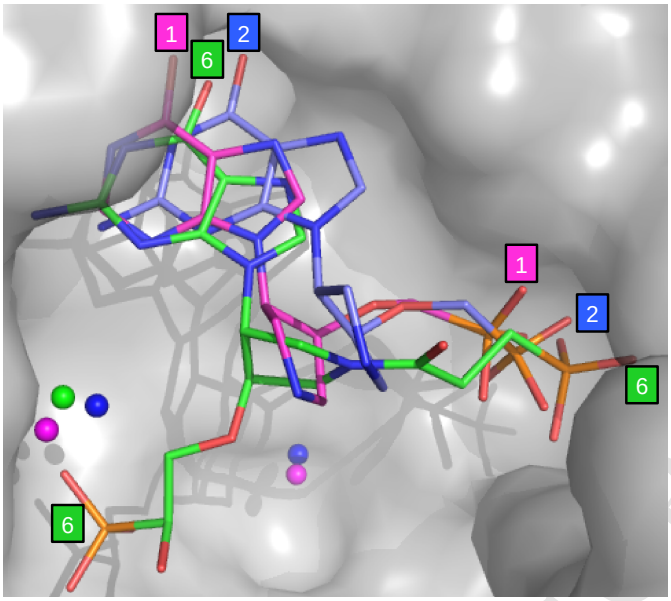

Fig. 11. Comparison of the binding modes of **1**, **2** and **6** in the active site of *Mt*HGPRT (subunit D). Connolly surface of the enzyme from the complex with **1** is overlaid. Inhibitors **1**, **2** and **6** have carbon atoms coloured as magenta, cyan and green, respectively. The location of the divalent metal ions in the three structures are shown in magenta (**1**; two magnesium ions), cyan (**2**; two magnesium ions) and green (**6**; one magnesium ion).

2.3.3. The pyrrolidine ring

The pyrrolidine ring covalently connects the three functional groups. Though the atoms in the ring do not make any interactions with active site residues (**Figs. 7**, **8** and **9**), the chemical structure of the ring itself is critical in placing these groups in the predicted binding sites.[28]

The presence of the rotatable bond between the N^9 atom of the purine ring and the C1′ atom of the pyrrolidine ring in **6**[19] allows for either one of the two phosphonate groups (attached at R^1 or R^2; **Fig. 2**) to be placed in the two areas in the active site able to bind a phosphate group *i.e.* the 5′-phosphate or the PP_i binding sites. In the *Mt*HGPRT.**6** complex, the phosphonate group attached to the nitrogen in the pyrrolidine ring (R^2) occupies the 5′-phosphate binding pocket in subunits B, C and D

(**Fig. 9B**). However, in subunit A, a second orientation occurs 40% of the time (**Fig. 9A**) with the phosphonate group at R^1 occupying the binding site of the 5′-phosphate group of GMP. It is this latter orientation that **6** adopts when it binds to human HGPRT (**Fig. 12B**).[19]

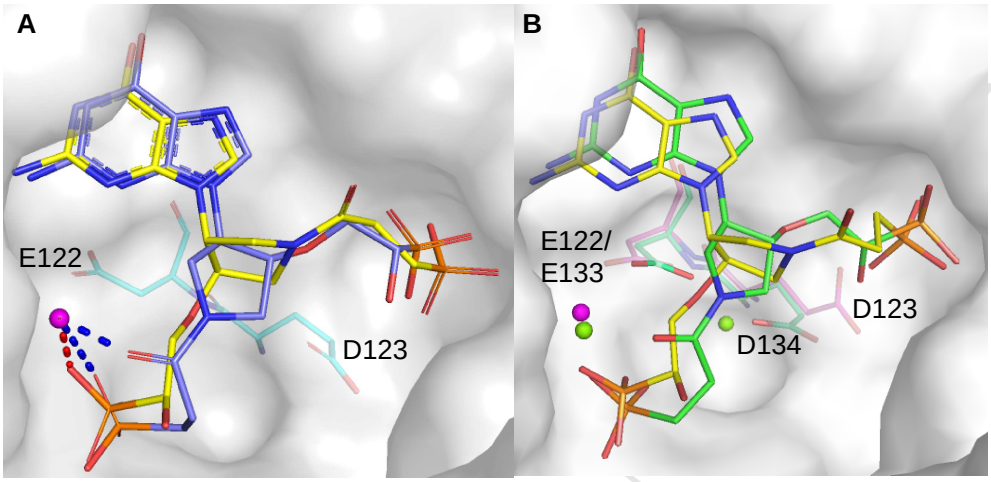

Fig. 12. Comparison of the binding modes of **6** in the active site of *Mt*HGPRT and human HGPRT. Connolly surface of *Mt*HGPRT is overlaid in both panels. (**A**) Superimposition of the two different orientations of **6** in subunit A of *Mt*HGPRT. There is only one magnesium ion (magenta) in this subunit. In the least favoured orientation of compound **6** (blue), this ion is coordinated to the carbonyl group in the linker and to one of the phosphonyl oxygens (blue dashes) while, in the most favoured (yellow), it is coordinated to a phosphonyl oxygen (red dashes). (**B**) Superimposition of *Mt*HGPRT.**6** (subunit B; yellow) with human HGPRT.**6** (green; PDB code: 5HIA).[19] Magenta is the single magnesium ion in the *Mt*HGPRT.**6** complex; green is the two magnesium ions in the human HGPRT.**6** complex. The two invariant ED residues (122-123 in *Mt*HGPRT and 133-134 in human HGPRT) are in magenta (*Mt*HGPRT.**6** complex) and green (human HGPRT.**6** complex). It is hypothesised that it is the movement of mobile loops in the two enzymes which determine how **6** binds in the active site.

2.3.4. The two phosphonate groups.

The 5′-phosphate binding pocket. The phosphonate group found in the predicted 5′-phosphate binding pocket when each of the three inhibitors binds to *Mt*HGPRT is surrounded by a flexible loop,

residues D126-T130 (**Figs. 7**, **8** and **9**). This phosphonate group pushes deepest into this pocket when the compounds exhibit the lowest K_i values *i.e.* **6** > **2** > **1** (**Table 1**; **Fig**. **11**). The location of this group when compounds **1** and **2** bind results in empty space at the bottom of this pocket which is filled by water molecules (**Figs. 7** and **8**). Thus, the third phosphonyl oxygen forms hydrogen bonds to three water molecules. This generates an extensive network of hydrogen bonds which helps to anchor the two inhibitors in the active site. One of these waters forms part of a series of hydrogen bonds to other water molecules one of which is coordinated to the magnesium atom that is liganded to E122 and D123 (**Figs**. **7** and **8**).

As the phosphonate group of **6** pushes deeper into the 5′-phosphate binding pocket (subunits B, C and D; **Fig. 9**), it occupies most of the available space in this cavity leaving no room for water molecules. It is possible that the changes in the hydrogen bond network due to the absence of water molecules could be one reason why the side chains of the ED residues have not been able to move the ligand to a magnesium ion as found in the *Mt*HGPRT.**1** and *Mt*HGPRT.**2** complexes.

In the *Mt*HGPRT.**6** complex, the flexible loop (D126-T130) is itself surrounded by two loops (K154-V162 and I171-D174) (**Fig**. **13**). Residues P155-H159 form an α-helix which joins two random coils (K154-P155 and H159–V162). In comparison, the corresponding loop in the human HGPRT.**6** complex, T167-V171, is a simply a random coil and is further away from the 5′-phosphate binding loop (**Fig. 13**). D137 acts as general acid/base in catalysis in human HGPRT[29] and D126 probably performs the same function in *Mt*HGPRT.[15] Thus, the OD atom of D137 forms a hydrogen bond with N^7 of the purine base in the transition state of catalysis. If the structure of the two *Mt*HGPRT.**6** complexes represents that prior to catalysis, then four bonds would have to be broken before D126 could move into position to form a hydrogen bond with the N^7 atom (**Fig. 13**). These are between the OD atom of D126 to OD1 (N173), to two OD atoms (D156) and between the OD1 atom of D156 and N173. In comparison, only one bond has to be broken in the human structure and this is

between OD of D137 and OE of R169 (**Fig**. **12**). This pattern of hydrogen bonds may contribute to the lower k_{cat} for *Mt*HGPRT.

The phosphonate group has to bend down into this pocket in the *Mt*HGPRT.**6** complex (**Fig. 13**). This suggests that the loops surrounding D126-T140 restrict the movement of the D126-T140 loop and, thus, the inhibitor itself has to adapt its shape to fit in this pocket.

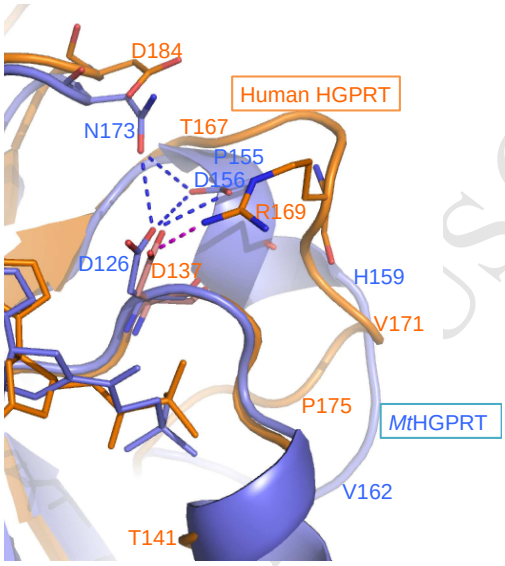

Fig. 13. Comparison of the structure of the 5′-phosphate binding pocket in the *Mt*HGPRT.**6** (blue) and human HGPRT.**6** (orange; PDB code, 5HUI)[19] complexes and the surrounding loop. The 5′-phosphate binding loop is DSGLT (126-130) in *Mt*HGPRT and DTGKT (137-141) in human HGPRT.

2.3.5. The pyrophosphate binding pocket

The addition of PP_i to the assay for *Mt*HGPRT together with the compounds **1** and **2** significantly decreases the K_i values (**Table 1**) suggesting that PP_i binds in the active site together with the inhibitor. The reaction mechanism of *Mt*HGPRT is reported to be ordered sequential[15] and, so, PP_i cannot enter the active site alone and has to exit before GMP/IMP in the forward reaction or after GMP/IMP in the reverse reaction. Superimposition of the structures of the *Mt*HGPRT.**1** and **2** complexes onto that of the human.**ImmGP**.**PP$_i$** structure[25] (**Figs**. **10A** and

10B) shows that one of the two PP_i molecules found in the active site of the *Mt*HGPRT complexes mimics that of pyrophosphate during the transition state of catalysis. The location of the second PP_i molecule is proposed to reflect its position immediately prior to, or just, after catalysis.

. **Figs. 10A** and **B** suggest that the β phosphate group of PP_i is the first to enter or leave the active site. The α phosphate group rotates around the phosphorus-oxygen bond resulting in this phosphorus atom moving by 3.7 Å. In all three complexes, the side chain of K66 points away from the active site and towards the adjacent subunit. This occurs even in subunits A and B of the *Mt*HGPRT.**2**.PP_i complex, where a single pyrophosphate molecule is present and is entering the site. In subunit A, one of the phosphoryl oxygens (α phosphate group; **Fig. 10B**) forms a hydrogen bond the NZ atom of K66. This hydrogen bond between one of the oxygen atom on the α phosphate group also occurs in subunits C and D of the *Mt*HGPRT.**1**.PP_i complex. This could suggest that, unlike human HGPRT, there is no rotation of the lysine side chain in *Mt*HGPRT (K66 in *Mt*HGPRT and K68 in human HGPRT) when PP_i enters the active site because, in the *Mt* enzyme, this side chain is already in position. This hypothesis was previously proposed based on the oligomeric states of *Mt*HGPRT.[30] The structures of *Mt*HGPRT in complex with **1** or **2** in the presence of PP_i appear to provide further validation for this proposition. In the unliganded structure of *Ec*HPRT, and in complex with IMP, the corresponding K residue is also rotated out of the PP_i binding site.[31] Thus, in this respect, the two bacterial enzymes could be similar and differ from human HGPRT.

In the *Mt*HGPRT.**1**.PP_i complex, one of the phosphoryl oxygens is located 3 Å away from the nitrogen atom in the pyrrolidine ring suggesting that pyrophosphate is helping the inhibitor to bind in its optimal location. This is consistent with the 27-fold derease in the K_i value which occurs in the presence of this second product of the reaction (**Table 1**).

2.3.6. The large mobile loop

In the human HGPRT, a large mobile loop (L100-G117) closes over the active site during catalysis. This is shown by the structure of human HGPRT (PDB code: 1BZY) in complex with a transition state analog, ImmGP. In *Mt*HGPRT, the corresponding residues are V90-L106 (**Fig. 6**). However, there are no structures of *Mt*HGPRT where this loop is "closed" so it is not proven if this loop does, or can, close. For human HGPRT, the amino acid residues in this loop are only visualized during the transition state of the catalytic reaction[25] but, for *Mt*HGPRT, the amino acid residues in the flexible loop are resolved in all three inhibitor complexes (**Table S1**). The only known crystal structure where this loop is closed just in the presence of an inhibitor that is not mimicking the transition state of the reaction is that of *Pf*HGXPRT in complex with an acyclic immucillin phosphonate plus pyrophosphate and magnesium.[26]

In the *Mt*HGPRT structures, an α-helix of five residues (S96-S100) is inserted in the random coil (**Figs. 14A** and **B**). For this loop to close over the active site during catalysis, this α-helix presumably would have to unravel and then re-form after the products are released. The Cα backbone would start to move to occupy an interim position such as the *Ec*HPRT.**1** structure (**Fig. 14B**)[31] before reaching its final conformation and location which is assumed to be completely over the active site as in the human HGPRT.ImmGP.PP_i complex.[25]

In all three structures of *Mt*HGPRT in complex with the inhibitors, the amino acids in the loop do not form any interactions with the inhibitor. Instead, they form hydrogen bonds with amino acid residues in adjacent subunits as has been observed previously in the *Mt*HGPRT.GMP complex.[13] The inter-subunit interactions may make it more difficult for the loop to fully close.

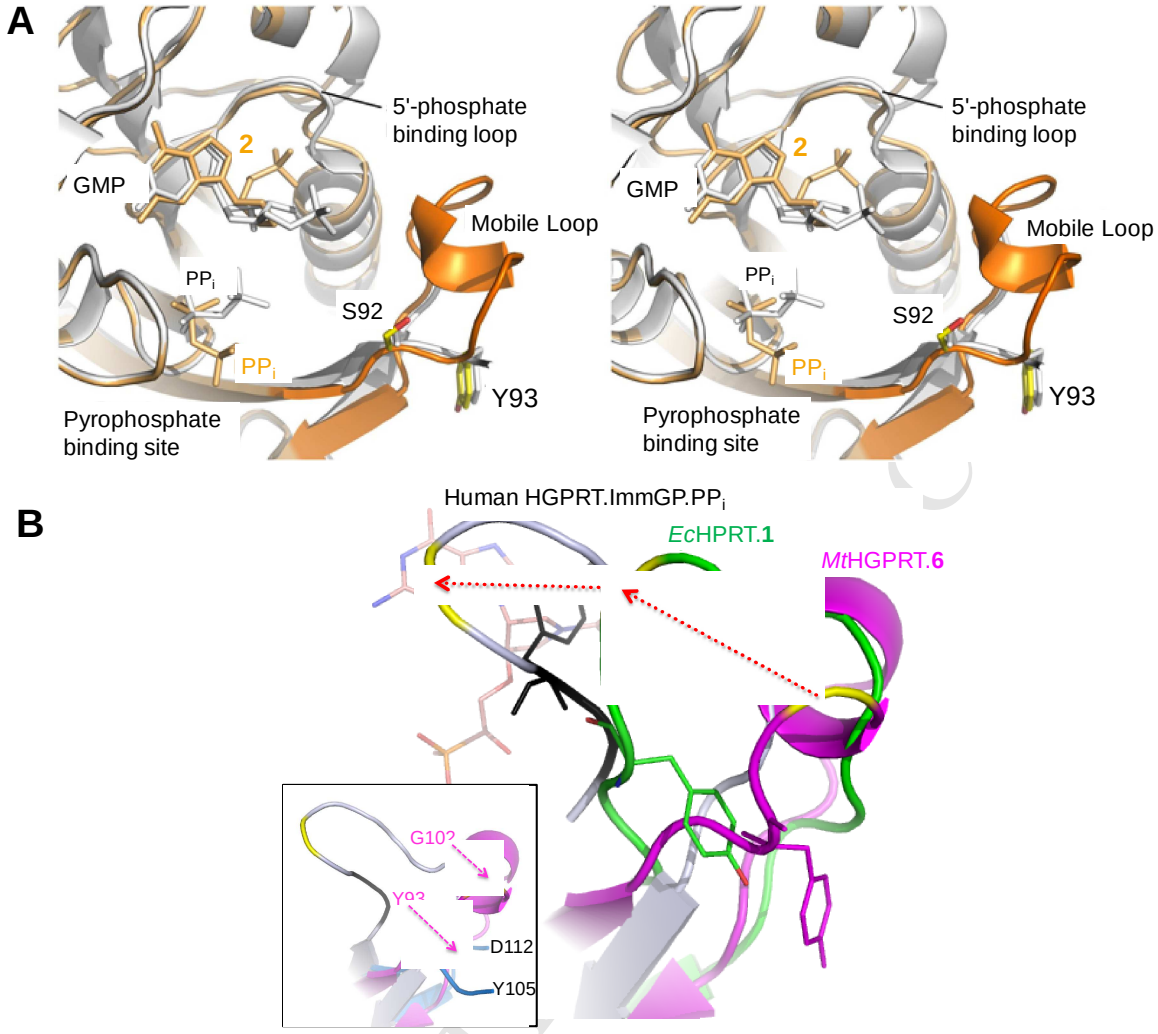

Fig. 14. Comparison of the large mobile loop structures in *Mt*HGPRT and human HGPRT. **A.** Structure of *Mt*HGPRT.**2**.PP_i (subunit A, orange) superimposed with the structure of *Mt*HGPRT.GMP.PP_i (PDB: 4RHT subunit A, white).[13] **B**. The movement of the large mobile loop. *Magenta*: *Mt*HGPRT.**6**, residues S91-R104. *Green*: *Ec*HPRT.**1** (PDB code: 5KNX), residues S91-R104.[31] *Grey*: Human HGPRT.ImmGP.PP_i (PDB code: 1BZY), residues K102-K114.[25] Y is the conserved tyrosine residue (*Mt*, Y93; *Ec*, Y74; human, Y104). The arrows show the distance between the position of three amino acid residues (yellow) in loop in the three structures: S95 (*Mt*HGPRT) to S76 (*Ec*HPRT) is 9.2 Å, and S76 (*Ec*HPRT) to N106 (human). **Insert:** The mobile loop in human HGPRT (*Blue*: PDB code: 5HIA)[19] and *Mt*HGPRT (magenta)

in complex with **6**. The "closed" position of this loop in the HGPRT.ImmGP.PP_i complex is shown for comparison.

2.4. In vitro *cell culture studies.*

The first step in assessing if potential compounds warrant further investigation and development as anti-TB chemotherapeutics is to assess their ability to arrest the growth of *Mt* in cell culture. As **6** is highly negatively charged at neutral pH, this restricts the ability of the compound to cross cell membranes. Therefore, for this type of drug, hydrophobic groups are rountinely attached to the phosphonate moieties to enhance delivery to the cell of interest.[32-33] In this instance, the tetra-(ethyl L-phenylalanine) tetraamide prodrug of **6** was chosen (**Fig. 15A**). Once within the cell, the attached groups are hydrolysed by constitutive enzymes to produce the active inhibitor, **6**, together with phenylalanine. This prodrug arrests the growth of *Mt* (H37Rv strain) with MIC_{90} values of 14 μM under conditions that mimic replicative growth (**Fig. 15B**). In latent TB, the mycobacteria lies dormant in caseous lesions of the lungs where there is little access to oxygen.[34-35] Therefore, to mimic the latent stage, the prodrug was tested against the growth of *Mt* H37Rv under hypoxic conditions resulting in an MIC_{90} of 29 μM (Figure **15B**), only a two-fold increase compared to the replicative stage. In the intramacrophage *Mt* H37Rv assay *in vitro*, the prodrug exhibited an MIC_{90} value of 85 μM. Against a mammalian cell line (A549), it exhibited a CC_{50} value of 132 ± 20 μM.

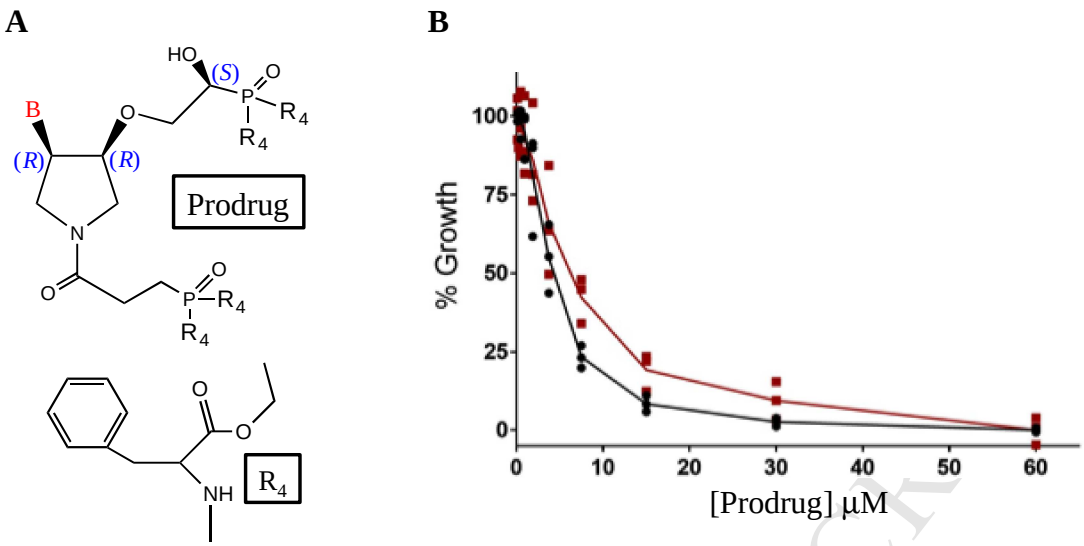

Fig. 15. Anti-TB activity of the tetra-(ethyl L-phenylalanine) tetraamide prodrug of **6** in *Mt* (H37Rv strain). **A.** Chemical structure of the prodrug. **B.** Inhibition of growth of *Mt* by the prodrug. The black dots represent the cell-based assay preformed under normal conditions while the red squares represent the assay results performed under hypoxic conditions.

Thus, the prodrug is active against *Mt* not only when it is in its replicative stage but also when it is in its dormant phase. This is a very desirable property for any potential anti-TB drug candidate.

Conclusions

The pyrrolidine nucleoside monophosphonates, [3*R*,4*S*]-(4-(hypoxanthin-9-yl)pyrrolidin-3-yl)-oxymethanephosphonic acid and [3*R*,4*S*]-(4-(guanin-9-yl)pyrrolidin-3-yl)oxymethanephosphonic acid, are micromolar inhibitors of the anti-TB drug target, hypoxanthine-guanine phosphoribosyltransferase. Crystal structures of *Mt*HGPRT in complex with these two inhibitors, plus PP_i, reveal the route whereby PP_i enters and leaves the active site prior to, or after, catalysis. They also show the location of this molecule during the transition state of the

reaction. The pyrrolidine nucleoside bisphosphonates (PNBPs) are the best inhibitors of *Mt*HGPRT yet discovered with K_i values between 40-60 nM. The X-ray crystal structures of *Mt*HGPRT and human HGPRT in complex with [3*R*,4*R*]-4-guanin-9-yl-3-((*S*)-2-hydroxy-2-phosphonoethyl)oxy-1-*N*-(phosphonopropionyl)pyrrolidine show the different binding modes in the two active sites. It is proposed that it is the movement and/or structures of flexible loops surrounding the active site that dictates how these compounds bind. To enhance cell permeability, a tetra-(ethyl L-phenylalanine) tetraamide prodrug of this compound was prepared. The first step in drug development is to test if the compound of interest is effective against TB in cell culture. This produg not only arrested the growth of TB in a virulent strain but an extra bonus in this study was the finding that the prodrug was also active against *Mt* during bacterial dormancy. This is a rare occurence for any potential anti-TB drug and a much sought-after property of such drugs. This prodrug is also effective against intramacrophage *Mt* H37Rv cells and has low cytotoxicity in human cell lines. Studies are now proposed to modify the inhibitor design based on the crystal structures and to improve the prodrug design specifically for TB cells as produgs of phosphonate compounds have yet to be designed to penetrate the TB cell membranes in particular. This data forms a solid foundation for the production of new anti-TB therapeutics.

3. Experimental

3.1. Synthesis and Analytical Chemistry

The chemical synthesis of compounds **1** and **2**[23] was performed according to previously published methods as was that of compounds **5**, **6**, and **8**.[19] The synthesis of the prodrug of **6** has been also reported.[19]

Unless stated otherwise, all solvents used were anhydrous. TLC was performed on silica gel pre-coated aluminium plates Silica gel/TLC-cards, UV 254 (Fluka) and compounds were detected by UV

light (254 nm), by heating (detection of dimethoxytrityl group; orange color), by spraying with 1% solution of ninhydrine to visualize amines, or by spraying with 1% solution of 4-(4-nitrobenzyl)pyridine in ethanol followed by heating and treating with gaseous ammonia (blue color of mono- and diesters of phosphonic acid). Preparative column chromatography was carried out on silica gel (40-60 µm; Fluka) and elution was performed at the flow rate of 40 ml/min. The following solvent systems were used for TLC and preparative chromatography: toluene-ethyl acetate 1:1 (T); chloroform-ethanol 9:1 (C1); ethyl acetate-acetone-ethanol-water 6:1:1:0.5 (H3); ethyl acetate-acetone-ethanol-water 4:1:1:1 (H1). The concentrations of solvent systems are stated in volume percent (% v/v). Purity of prepared compounds was determined by LC-MS performed on Waters Auto Purification System with 2545 Quaternary Gradient Module and 3100 Single Quadrupole Mass Detector using LUNA C18 column (Phenomenex, 100 x 4.6 mm, 3 µm) at a flow rate of 1 ml/min. Purity of prepared final compounds was > 95%. Typical conditions were: mobile phase, A – 50 mM NH_4HCO_3; B - 50 mM NH_4HCO_3 in 50% aq. CH_3CN; C – CH_3CN; A→B/10 min, B→C/10 min, C/5 min. Preparative reverse phase HPLC (rpHPLC) was performed on a LC5000 Liquid Chromatograph (INGOS-PIKRON, CR) using a Luna C18 (2) column (250 x 21.2 mm, 5 µm) at a flow rate of 10 ml/min by gradient elution of methanol in 0.1M TEAB pH 7.5 (A = 0.1M TEAB; B = 0.1M TEAB in 50% aq. methanol; C = methanol) or without buffer. Final compounds were lyophilized from water. Mass spectra were recorded on LTQ Orbitrap XL (Thermo Fisher Scientific) using ESI ionization. NMR spectra were measured on Bruker AVANCE 400 (^{1}H at 400 MHz, ^{13}C at 100.6 MHz), Bruker AVANCE 500 and Varian UNITY 500 (^{1}H at 500 MHz, ^{13}C at 125.8 MHz) spectrometers. D_2O (reference (dioxane) = ^{1}H 3.75 ppm, ^{13}C 69.3 ppm. Chemical shifts (in ppm, d scale) were referenced to TMS as an internal standard; coupling constants (*J*) are given in Hz. All intermediates were determined by LC-MS. 1-*N*-Boc-3-dimethoxytrityloxy-4-hydroxypyrrolidines (all configurations) were prepared according to a previously established procedure.

*3.2. [3S,4R]-4-Hypoxanthin-9-yl-3-phosphonoethyloxy-1-N-(phosphonopropionyl)pyrrolidine (**3**)*

Title compound was prepared using the same methodology as described previously[19], starting from [3*S*,4*S*]-3-dimethoxytrityloxy-1-*N*-Boc-4-hydroxypyrrolidine (0.9 g, 1.71 mmol) in 8% overall yield (79.5 mg, 0.14 mmol) in the form of white amorphous solid.

~ 6:7 mixture of rotamers A:B

^{1}H NMR (500.0 MHz, D_2O, ref(dioxane) = 3.75 ppm, 25 °C): 1.58-1.81 (m, 4H, $OCH_2C\mathbf{H_2}$P-A,B); 1.81 – 1.91 (m, 4H, $COCH_2C\mathbf{H_2}$P-A,B); 2.59 – 2.70 (m, 4H, $COC\mathbf{H_2}CH_2$P-A,B); 3.46-3.61 (m, 2H, $OCH_aC\mathbf{H_b}CH_2$P-A,B); 3.68-3.78 (m, 3H, H-5′b-A, $OC\mathbf{H_a}CH_bCH_2$P-A,B); 3.82 (dd, 1H, J_{gem} = 11.9, $J_{5'b,4'}$ = 4.3, H-5′b-B); 3.84 (dd, 1H, J_{gem} = 13.2, $J_{5'a,4'}$ = 5.4, H-5′a-A); 4.05 (dd, 1H, J_{gem} = 12.6, $J_{2'b,3'}$ = 6.9, H-2′b-B); 4.07 (dd, 1H, J_{gem} = 11.9, $J_{5'a,4'}$ = 5.5, H-5′a-B); 4.13 (dd, 1H, J_{gem} = 12.6, $J_{2'b,3'}$ = 7.7, H-2′a-B); 4.24 (dd, 1H, J_{gem} = 11.2, $J_{2'b,3'}$ = 7.6, H-2′b-A); 4.29 (dd, 1H, J_{gem} = 11.2, $J_{2'a,3'}$ = 7.6, H-2′a-A); 4.50 (ddd, 1H, $J_{4',5'}$ = 5.4, 3.7, $J_{4',3'}$ = 4.7, H-4′-A); 4.56 (ddd, 1H, $J_{4',5'}$ = 5.5, 4.3, $J_{4',3'}$ = 4.8, H-4′-B); 5.40 (ddd, 1H, $J_{3',2'}$ = 7.6, 6.9, $J_{3',4'}$ = 4.8, H-3′-B); 5.21 (td, 1H, $J_{3',2'}$ = 7.6, $J_{3',4'}$ = 4.6, H-3′-A); 8.22 (s, 2H, H-2-A,B); 8.25 (s, 1H, H-8-B); 8.28 (s, 1H, H-8-A).

^{13}C NMR (125.7 MHz, D_2O, ref(dioxane) = 69.30 ppm, 25 °C): 25.95 (d, $J_{C,P}$ = 134.7, $COCH_2\mathbf{C}H_2$P-B); 25.99 (d, $J_{C,P}$ = 134.6, $COCH_2\mathbf{C}H_2$P-A); 31.28 (d, $J_{C,P}$ = 2.4, $CO\mathbf{C}H_2CH_2$P-B); 31.36 (d, $J_{C,P}$ = 2.4, $CO\mathbf{C}H_2CH_2$P-A); 31.70 (d, $J_{C,P}$ = 129.1, $OCH_2\mathbf{C}H_2$P-B); 31.71 (d, $J_{C,P}$ = 129.1, $OCH_2\mathbf{C}H_2$P-A); 50.25 (CH_2-2′-B); 50.92 (CH_2-2′-A); 52.13 (CH_2-5′-A); 52.82 (CH_2-5′-B); 56.87 (CH-3′-B); 57.90 (CH-3′-A); 69.13 (d, $J_{C,P}$ = 2.4, $O\mathbf{C}H_2CH_2$P-A); 69.32 (d, $J_{C,P}$ = 2.5, $O\mathbf{C}H_2CH_2$P-B); 78.93 (CH-4′-A); 80.09 (CH-4′-B); 125.79 (C-5-A); 125.84 (C-5-B); 143.74 (CH-8-B); 143.89 (CH-8-A); 148.55 (CH-2-A,B); 152.04 (C-4-A); 152.09 (C-4-B); 161.41 (C-6-A,B); 177.21 (d, $J_{C,P}$ = 17.9, NCO-A); 177.29 (d, $J_{C,P}$ = 17.9, NCO-B).

^{31}P[^{1}H] NMR (202.3 MHz, D_2O, ref (external H_3PO_4) = 0 ppm, 25 °C): 19.53 (PCH_2CH_2O-A); 19.58 (PCH_2CH_2O-B); 23.20 (PCH_2CH_2CO-A); 23.29 (PCH_2CH_2CO-B).

HRMS (ESI-) for $C_{14}H_{20}N_5O_9P_2$ $(M-H)^-$: calcd 464.07417, found 464.07417.

*3.3. [3S,4R]-4-Guanin-9-yl-3-phosphonoethyloxy-1-N-(phosphonopropionyl)pyrrolidine (**4**)*

Title compound was prepared using the same methodology described previously,[19] starting from [3*S*,4*S*]-3-dimethoxytrityloxy-1-*N*-Boc-4-hydroxypyrrolidine (1.18 g, 2,32 mmol) in 7% overall yield (291 mg, 0.51 mmol) in the form of white amorphous solid.

~ 6:7 mixture of rotamers A:B

^{1}H NMR (500.0 MHz, D_2O, ref(dioxane) = 3.75 ppm, 25 °C): 1.64-1.83 (m, 4H, $OCH_2C\mathbf{H_2}$P-A,B); 1.83 – 1.91 (m, 4H, $COCH_2C\mathbf{H_2}$P-A,B); 2.60 – 2.67 (m, 4H, $COC\mathbf{H_2}CH_2$P-A,B); 3.52-3.83 (m, 7H, H-5′-A, H-5′b-B, $OC\mathbf{H_2}CH_2$P-A,B); 3.96 (dd, 1H, J_{gem} = 12.6, $J_{2'b,3'}$ = 7.1, H-2′b-B); 4.02 (dd, 1H, J_{gem} = 11.9, $J_{5'a,4'}$ = 5.4, H-5′a-B); 4.07 (dd, 1H, J_{gem} = 12.6, $J_{2'b,3'}$ = 7.7, H-2′a-B); 4.15 (dd, 1H, J_{gem} = 11.2, $J_{2'b,3'}$ = 7.6, H-2′b-A); 4.23 (dd, 1H, J_{gem} = 11.2, $J_{2'a,3'}$ = 7.6, H-2′a-A); 4.44 (ddd, 1H, $J_{4',5'}$ = 5.1, 3.7, $J_{4',3'}$ = 4.6, H-4′-A); 4.50 (dt, 1H, $J_{4',5'}$ = 5.4, 4.6, $J_{4',3'}$ = 4.6, H-4′-B); 5.15 (ddd, 1H, $J_{3',2'}$ = 7.7, 7.1, $J_{3',4'}$ = 4.6, H-3′-B); 5.21 (td, 1H, $J_{3',2'}$ = 7.6, $J_{3',4'}$ = 4.6, H-3′-A); 7.89 (s, 1H, H-8-B); 7.93 (s, 1H, H-8-A).
^{13}C NMR (125.7 MHz, D_2O, ref(dioxane) = 69.30 ppm, 25 °C): 25.92 (d, $J_{C,P}$ = 134.7, $COCH_2\mathbf{C}H_2$P-B); 25.95 (d, $J_{C,P}$ = 134.7, $COCH_2\mathbf{C}H_2$P-A); 31.21 (d, $J_{C,P}$ = 2.4, $CO\mathbf{C}H_2CH_2$P-B); 31.32 (d, $J_{C,P}$ = 2.4, $CO\mathbf{C}H_2CH_2$P-A); 31.65 (d, $J_{C,P}$ = 129.0, $OCH_2\mathbf{C}H_2$P-B); 31.67 (d, $J_{C,P}$ = 129.0, $OCH_2\mathbf{C}H_2$P-A); 50.08 (CH_2-2′-B); 50.82 (CH_2-2′-A); 52.11 (CH_2-5′-A); 52.76 (CH_2-5′-B); 56.02 (CH-3′-B); 57.13 (CH-3′-A); 69.17 (d, $J_{C,P}$ = 2.5, $O\mathbf{C}H_2CH_2$P-A); 69.37 (d, $J_{C,P}$ = 25.0, $O\mathbf{C}H_2CH_2$P-B); 78.88 (CH-4′-A); 80.05 (CH-4′-B); 118.26 (C-5-A); 118.29 (C-5-B); 141.14 (CH-8-B); 141.34 (CH-8-A); 154.71 (C-4-A); 154.76 (C-4-B); 156.48 (C-2-A,B); 161.68 (C-6-A,B); 177.13 (d, $J_{C,P}$ = 17.8, NCO-A); 177.17 (d, $J_{C,P}$ = 17.8, NCO-B).
^{31}P [^{1}H] NMR (202.3 MHz, D_2O, ref (external H_3PO_4) = 0 ppm, 25 °C): 19.73 (PCH_2CH_2O-A); 19.75 (PCH_2CH_2O-B); 23.32 (PCH_2CH_2CO-A); 23.39 (PCH_2CH_2CO-B).

HRMS (ESI-) for $C_{14}H_{21}N_6O_9P_2$ $(M-H)^-$: calcd 479.08507, found 479.08478.

*3.4. [3R,4R]-4-Hypoxanthin-9-yl-3-((R)-2-hydroxy-2-phosphonoethyl)oxy-1-N-(phosphonopropionyl)pyrrolidine (**7**)*

Title compound was prepared using the same methodology as described previously, starting from diisopropyl ((*R*)-1-*tert*-butyldimethylsilyloxy-2-(((3*R*,4*S*)-1-*N*-boc-4-dimethoxytrityloxypyrrolidin-3-yl)oxy)ethyl)phosphonate (compounds **10-R**[19]) (0.31 g, 0.59 mmol) in overall 31% yield (56.9 mg, 0.1 mmol) in the form of white amorphous solid.

~ 6:7 mixture of rotamers A:B

^{1}H NMR (500.0 MHz, D_2O, ref(dioxane) = 3.75 ppm, 25 °C): 1.81 – 1.94 (m, 4H, $COCH_2C\mathbf{H_2}$P-A,B); 2.60 – 2.71 (m, 4H, $COC\mathbf{H_2}CH_2$P-A,B); 3.64 – 3.78 (m, 3H, H-5′b-A, $OCH_a\mathbf{H_b}$CH(OH)P-A,B); 3.84 (dd, 1H, J_{gem} = 12.1, $J_{5'b,4'}$ = 3.6, H-5′b-B); 3.85-4.03 (m, 5H, H-5′a-A, C**H**(OH)P-A,B,

OC**H$_a$**H$_b$CH(OH)P-A,B); 4.08 (dd, 1H, J_{gem} = 13.3, $J_{2'b,3'}$ = 4.5, H-2′b-B); 4.10-4.21 (m, 2H, H-2′a,5′a-B); 4.22 (dd, 1H, J_{gem} = 12.2, $J_{2'b,3'}$ = 4.7, H-2′b-A); 4.37 (dd, 1H, J_{gem} = 12.2, $J_{2'a,3'}$ = 7.3, H-2′a-A); 4.60 (dt, 1H, $J_{4',5'}$ = 5.9, 4.0, $J_{4',3'}$ = 4.0, H-4′-A); 4.65 (ddd, 1H, $J_{4',5'}$ = 5.9, 3.6, $J_{4',3'}$ = 3.9, H-4′-B); 5.25 (ddd, 1H, $J_{3',2'}$ = 7.2, 4.5, $J_{3',4'}$ = 3.9, H-3′-B); 5.33 (ddd, 1H, $J_{3',2'}$ = 7.3, 4.7, $J_{3',4'}$ = 4.0, H-3′-A); 8.12 (s, 1H, H-8-B); 8.17 (s, 1H, H-8-A); 8.20 (s, 2H, H-2-A,B).

^{13}C NMR (125.7 MHz, D_2O, ref(dioxane) = 69.30 ppm, 25 °C): 25.93 (d, $J_{C,P}$ = 134.8, COCH$_2$**C**H$_2$P-A,B); 31.31 (d, $J_{C,P}$ = 2.4, CO**C**H$_2$CH$_2$P-A); 31.41 (d, $J_{C,P}$ = 2.4, CO**C**H$_2$CH$_2$P-B); 50.79 (CH$_2$-2′-B); 51.67 (CH$_2$-2′-A); 52.15 (CH$_2$-5′-A); 53.03 (CH$_2$-5′-B); 60.04 (CH-3′-B); 61.22 (CH-3′-A); 71.60 (d, $J_{C,P}$ = 150.7, CH(OH)P-A,B); 74.10 (d, $J_{C,P}$ = 11.0, O**C**H$_2$CH(OH)P-A); 74.19 (d, $J_{C,P}$ = 11.0, O**C**H$_2$CH(OH)P-B); 82.59 (CH-4′-A); 83.88 (CH-4′-B); 126.45 (C-5-A); 126.49 (C-5-B); 142.64 (CH-8-B); 142.78 (CH-8-A); 148.52 (CH-2-A,B); 151.67 (C-4-A,B); 161.37 (C-6-A,B); 177.12 (d, $J_{C,P}$ = 17.9, NCO-A); 177.21 (d, $J_{C,P}$ = 17.9, NCO-B).

^{31}P[^{1}H] NMR (202.3 MHz, D_2O, ref (external H_3PO_4) = 0 ppm, 25 °C): 15.17 (PCH(OH)CH$_2$O-A); 15.19 (PCH(OH)CH$_2$O-B); 23.33 (PCH$_2$CH$_2$CO-A); 23.39 (PCH$_2$CH$_2$CO-B). $C_{14}H_{20}N_5O_{10}P_2$ $(M-H)^-$: calcd 480.06909, found 480.06833.

3.5 Expression and purification of MtHGPRT

Recombinant *Mt*HGPRT was expressed and purified as previously described.[13] The enzyme was subsequently stored in 0.1 M Tris-HCl, 12 mM $MgCl_2$, pH 7.4, 200 μM *P*Rib-*PP* at −80 °C where it is stable for > 2 years.

3.6. Determination of K_i values

Enzyme activity was determined using a continuous spectrophotometric assay, by measuring the conversion of guanine to GMP at 257.5 nm ($\Delta\varepsilon$ = 5816.5 M^{-1} cm^{-1}). The K_i values were determined in 0.01 M phosphate buffer, 12 mM $MgCl_2$, pH 7.4. The concentration of guanine was fixed at 60 μM and the concentration of the second substrate *P*Rib-*PP* varying from 100−1500 μM depending on the $K_{m(app)}$ in the presence of the inhibitor. The concentration of inhibitor in the assays ranged from 80 nM to 6.6 μM, depending upon the potency of the particular compound. K_i values were calculated using

Prism4 (GraphPad Software, Inc., La Jolla, CA). For pyrophosphate, $K_{i(app)}$ was calculated using the equations $v=V_{max}[S]_o/[S]_o+K_{m(app)}$ and $K_{m(app)}=K_m(1+ [I]/ K_{i(app)})$.

3.7. Crystallization

Crystals were obtained using the hanging drop vapour diffusion method. The concentration of protein was 8 mg mL^{-1} and the concentration of inhibitor was 3.3 mM for **1**, 1.7 mM for **2** (with 1.9 mM of pyrophosphate) and 0.98 mM for **6**. The well solution for three complexes were: **1** and **2**, 20% PEG8000, 0.1 M Tris-HCl pH 8.5 and 0.2 M $MgCl_2$; **6** was 0.2 M Li_2SO_4, 0.1 M Sodium acetate pH 4.5 and 30% PEG8000. The drop consisted of an equal volume of well solution and protein inhibitor complex. Prior to data collection, crystals of *Mt*HGPRT.**2** and *Mt*HGPRT.**6** complex were transferred to a solution that contained well solution, 20% glycerol and inhibitor with final concentration of 2.2 mM and 4.9 mM, respectively. For compound **1**, no cryoprotection was required. Crystals were cryo-cooled in liquid nitrogen and transported to the Australian Synchrotron where they were robotically placed in a cryostream (100K) on beamline MX1. All X-ray data were collected remotely by Blu-Ice.[36] Data were merged and scaled using XDS.[37] The structures were solved by molecular replacement in PHASER,[38] within PHENIX 1.7.3,[39] using the *Mt*HGPRT.GMP complex (PDB: 4RHT) as the search model. Subsequent refinement and model building was with PHENIX 1.7.3[39] and COOT 0.7,[40] respectively. The structural restraints file for the inhibitors were generated by PRODRG2 Dundee server.[41]

3.8. Mt inhibition during in vitro assay

The potency of the inhibitors was measured by a resazurin reduction microplate assay, as previously described,[42-43] with some alterations. Virulent *Mt* H37Rv was grown in Middlebrook 7H9 broth medium supplemented with 10% ADC, 0.5% glycerol and 0.02% tyloxapol. Cultures were grown at 37 °C to mid-exponential phase (OD_{600} 0.4-0.8) and diluted to OD_{600} 0.002 in 7H9S media (Middlebrook 7H9 with 10% ADC, 0.5% glycerol, 0.75% tween-80, 1% tryptone). 96-well microtitre plates were

setup with 100 µl of inhibitors, serially diluted into 7H9S media. 100 µl of diluted *Mt*, representing ~2x10^4 CFU/mL was added to each well. Plates were incubated for five days at 37 °C. 42.5 µl of resazurin solution (30 µl of 0.02% resazurin, 12.5 µl of 20% Tween 80) was added to each well. Fluorescence was measured 24h later on a FluoroStar Omega fluorescent plate reader (BMG) with an excitation wavelength of 530 nm and an emission wavelength of 590 nm. Changes in fluorescence relative to positive control wells (H37Rv with no inhibitor) minus negative control wells (no H37Rv) were plotted for determination of MIC_{90}. Hypoxic conditions are exactly the same except the plates were placed in a hypoxic chamber (0.1% O_2). Completed hypoxic assay was read after 48 hrs post resazurin addition in aerobic conditions. Control assays with isoniazid were preformed in parallel to hypoxic killing assays. A loss of killing potential of isoniazid is a reliable indicator of bacterial dormancy.

3.9. Mt inhibition assay in macrophages

Human monocytic THP-1 cells were cultured in RPMI 1640 supplemented with 10% FBS, 0.05 mM β-mercaptoethanol and 2 mM glutamine, and incubated at 37 °C/5% CO_2. For infection experiments, THP-1 (5x10^5 cells/mL) were plated into 96-well plates in complete RPMI media containing 50 ng/ml phorbol 12-myristate 13-acetate (PMA, Sigma Chemical Co, St. Louis, MO) for differentiation to macrophages (incubated at 37 °C/5% CO_2). After 72 h, supernatants were removed and mCherry expressing, fluorescent *H37Rv* in RPMI media was used to infect the THP-1 cells at a Multiplicity of Infection (MOI) of 1:1 (1 bacteria/1 cell) for 2 h (37 °C/5% CO_2). Cells were then washed two times with fresh complete RPMI media to remove extracellular bacilli. The prodrug (**Fig. 15A**) was then added to infected macrophages at concentrations ranging from 250 µM to 0.5 µM and incubated at 37 °C and 5% CO_2 for 4 days, and fluorescence was then recorded.

3.10. Cytotoxicity assays in human cell lines

Human lung carcinoma A549 cells were seeded in 96-well plates at 7500 cells per well, and on the next day the compounds were added in serial dilutions. After four days incubation at 37 °C, the cells were trypsinized, then counted with a Coulter Counter apparatus. The CC_{50} or 50% cytostatic concentration, defined as the compound concentration producing 50% inhibition of cell proliferation as compared to the no compound control, was calculated by extrapolation assuming a semi-log dose-response effect.

Acknowledgements

The initial crystallographic conditions were determined using the Mosquito and Rock Imager facilities at the University of Queensland Remote-Operation Crystallization and X-ray Diffraction facility (UQROCX). Measurements were made at the MX1 beamline, Australian Synchrotron, Clayton, Victoria with the assistance of Tom Caradoc-Davies. The views expressed here are those of the authors and not necessarily those of the Australian Synchrotron. This work was supported by funds from the National Health and Medical Research Council (Grant No. 1147368), by the subvention for development of research organization (Institute of Organic Chemistry and Biochemistry, RVO 61388963), Czech ministry of health (Grant No.17-29680A to D.R.), and Czech Science Foundation (Grant No. 15-11711S to D.R.).

Supplementary Tables

Table S1. Data collection and refinement statistics for the *Mt*HGPRT.inhibitor complexes.

Table S2. RMSD values (Å) for the *Mt*HGPRT complexes after superimposition of the C*α* atoms.

Table S3. Molecular Strings.

The atomic coordinates and structure factors for the *Mt*HGPRT in complexes with compound have been deposited with the Protein Data Bank. Authors will release the atomic coordinates and experimental data upon article publication. For the *Mt*HGPRT.**1**.**PP$_i$** complex, the PDB code is 5KNP, for the *Mt*HGPRT.**1**.**PP$_i$** complex, the code is 5KNQ and for the *Mt*HGPRT.**6** complex, the PDB code

is 5KNY.

References

1. Koch, R., Classics in infectious diseases. The etiology of tuberculosis: Robert Koch. Berlin, Germany 1882. *Rev. Infect. Dis.* **1982,** *4* (6), 1270-1274.

2. WHO, *Global Tuberculosis Report* **2017**.

3. Zumla, A.; Raviglione, M.; Hafner, R.; von Reyn, C. F., Tuberculosis. *N. Engl. J. Med.* **2013,** *368* (8), 745-755.

4. Beena; Rawat, D. S., Antituberculosis drug research: a critical overview. *Med. Res. Rev.* **2013,** *33* (4), 693-764.

5. Jain, A.; Mondal, R., Extensively drug-resistant tuberculosis: current challenges and threats. *FEMS. Immunol. Med. Microbiol.* **2008,** *53* (2), 145-150.

6. Fox, G. J.; Dobler, C. C.; Marais, B. J.; Denholm, J. T., Preventive therapy for latent tuberculosis infection-the promise and the challenges. *Int. J. Infect. Dis.* **2017,** *56*, 68-76.

7. Filippini, P.; Iona, E.; Piccaro, G.; Peyron, P.; Neyrolles, O.; Fattorini, L., Activity of drug combinations against dormant *Mycobacterium tuberculosis*. *Antimicrob. Agents Chemother.* **2010,** *54* (6), 2712-2715.

8. Fox, G. J.; Menzies, D., A review of the evidence for using bedaquiline (TMC207) to treat multi-drug resistant tuberculosis. *Infect. Dis. Ther.* **2013,** *2* (2), 123-44.

9. Maryandyshev, A.; Pontali, E.; Tiberi, S.; Akkerman, O.; Ganatra, S.; Sadutshang, T. D.; Alffenaar, J. W.; Amale, R.; Mullerpattan, J.; Topgyal, S.; Udwadia, Z. F.; Centis, R.; D'Ambrosio, L.; Sotgiu, G.; Migliori, G. B., Bedaquiline and delamanid combination treatment of 5 patients with pulmonary extensively drug-resistant tuberculosis. *Emerg. Infect. Dis.* **2017,** *23* (10), 1718-1721.

10. Borisov, S. E.; Dheda, K.; Enwerem, M.; Romero Leyet, R.; D'Ambrosio, L.; Centis, R.; Sotgiu, G.; Tiberi, S.; Alffenaar, J. W.; Maryandyshev, A.; Belilovski, E.; Ganatra, S.; Skrahina, A.; Akkerman, O.; Aleksa, A.; Amale, R.; Artsukevich, J.; Bruchfeld, J.; Caminero, J. A.; Carpena Martinez, I.; Codecasa, L.; Dalcolmo, M.; Denholm, J.; Douglas, P.; Duarte, R.; Esmail, A.; Fadul, M.;

Filippov, A.; Davies Forsman, L.; Gaga, M.; Garcia-Fuertes, J. A.; Garcia-Garcia, J. M.; Gualano, G.; Jonsson, J.; Kunst, H.; Lau, J. S.; Lazaro Mastrapa, B.; Teran Troya, J. L.; Manga, S.; Manika, K.; Gonzalez Montaner, P.; Mullerpattan, J.; Oelofse, S.; Ortelli, M.; Palmero, D. J.; Palmieri, F.; Papalia, A.; Papavasileiou, A.; Payen, M. C.; Pontali, E.; Robalo Cordeiro, C.; Saderi, L.; Sadutshang, T. D.; Sanukevich, T.; Solodovnikova, V.; Spanevello, A.; Topgyal, S.; Toscanini, F.; Tramontana, A. R.; Udwadia, Z. F.; Viggiani, P.; White, V.; Zumla, A.; Migliori, G. B., Effectiveness and safety of bedaquiline-containing regimens in the treatment of MDR- and XDR-TB: a multicentre study. *Eur. Respir. J.* **2017,** *49* (5).

11. Hu, Y. Q.; Zhang, S.; Zhao, F.; Gao, C.; Feng, L. S.; Lv, Z. S.; Xu, Z.; Wu, X., Isoniazid derivatives and their anti-tubercular activity. *Eur. J. Med. Chem.* **2017,** *133*, 255-267.

12. Griffin, J. E.; Gawronski, J. D.; Dejesus, M. A.; Ioerger, T. R.; Akerley, B. J.; Sassetti, C. M., High-resolution phenotypic profiling defines genes essential for mycobacterial growth and cholesterol catabolism. *PLoS Pathog* **2011,** *7* (9), e1002251.

13. Eng, W. S.; Hockova, D.; Spacek, P.; Janeba, Z.; West, N. P.; Woods, K.; Naesens, L. M.; Keough, D. T.; Guddat, L. W., First crystal structures of M*ycobacterium tuberculosis* 6-oxopurine phosphoribosyltransferase: Complexes with GMP and pyrophosphate and with acyclic nucleoside phosphonates whose prodrugs have antituberculosis activity. *J. Med. Chem.* **2015,** *58* (11), 4822-4838.

14. Biazus, G.; Schneider, C. Z.; Palma, M. S.; Basso, L. A.; Santos, D. S., Hypoxanthine-guanine phosphoribosyltransferase from *Mycobacterium tuberculosis* H37Rv: cloning, expression, and biochemical characterization. *Protein Expr. Purif.* **2009,** *66* (2), 185-190.

15. Patta, P. C.; Martinelli, L. K. B.; Rotta, M.; Abbadi, B. L.; Santos, D. S.; Basso, L. A., Mode of action of recombinant hypoxanthine-guanine phosphoribosyltransferase from *Mycobacterium tuberculosis*. *Rsc Adv.* **2015,** *5* (91), 74671-74683.

16. Xu, Y.; Eads, J.; Sacchettini, J. C.; Grubmeyer, C., Kinetic mechanism of human hypoxanthine-guanine phosphoribosyltransferase: Rapid phosphoribosyl transfer chemistry. *Biochemistry* **1997,** *36* (12), 3700-3712.

17. Keough, D. T.; Skinner-Adams, T.; Jones, M. K.; Ng, A. L.; Brereton, I. M.; Guddat, L. W.; de Jersey, J., Lead compounds for antimalarial chemotherapy: Purine base analogs discriminate between human and *P. falciparum* 6-oxopurine phosphoribosyltransferases. *J. Med. Chem.* **2006,** *49* (25), 7479-7486.

18. De Clercq, E.; Holý, A., Acyclic nucleoside phosphonates: A key class of antiviral drugs. *Nat Rev Drug Discov* **2005,** *4* (11), 928-940.

19. Keough, D. T.; Rejman, D.; Pohl, R.; Zbornikova, E.; Hockova, D.; Croll, T.; Edstein, M. D.; Birrell, G. W.; Chavchich, M.; Naesens, L. M. J.; Pierens, G. K.; Brereton, I. M.; Guddat, L. W., Design of *Plasmodium vivax* hypoxanthine-guanine phosphoribosyltransferase inhibitors as potential antimalarial therapeutics. *ACS Chem. Biol.* **2017,** *13* (1), 82-90.

20. Keough, D. T.; Spacek, P.; Hockova, D.; Tichy, T.; Vrbkova, S.; Slavetinska, L.; Janeba, Z.; Naesens, L.; Edstein, M. D.; Chavchich, M.; Wang, T. H.; de Jersey, J.; Guddat, L. W., Acyclic nucleoside phosphonates containing a second phosphonate group are potent inhibitors of 6-oxopurine phosphoribosyltransferases and have antimalarial activity. *J. Med. Chem.* **2013,** *56* (6), 2513-2526.

21. Keough, D. T.; Hocková, D.; Holý, A.; Naesens, L. M.; Skinner-Adams, T. S.; de Jersey, J.; Guddat, L. W., Inhibition of hypoxanthine-guanine phosphoribosyltransferase by acyclic nucleoside phosphonates: A new class of antimalarial therapeutics. *J Med Chem* **2009,** *52* (14), 4391-4399.

22. Keough, D. T.; Hockova, D.; Rejman, D.; Spacek, P.; Vrbkova, S.; Krecmerova, M.; Eng, W. S.; Jans, H.; West, N. P.; Naesens, L. M.; de Jersey, J.; Guddat, L. W., Inhibition of the *Escherichia coli* 6-oxopurine phosphoribosyltransferases by nucleoside phosphonates: potential for new antibacterial agents. *J. Med. Chem.* **2013,** *56* (17), 6967-6984.

23. Pohl, R.; Postova Slavetinska, L.; Eng, W. S.; Keough, D. T.; Guddat, L. W.; Rejman, D., Synthesis, conformational studies, and biological properties of phosphonomethoxyethyl derivatives of nucleobases with a locked conformation via a pyrrolidine ring. *Org. Biomol. Chem.* **2015,** *13* (16), 4693-4705.

24. Shi, W.; Li, C. M.; Tyler, P. C.; Furneaux, R. H.; Cahill, S. M.; Girvin, M. E.; Grubmeyer, C.; Schramm, V. L.; Almo, S. C., The 2.0 Å structure of malarial purine phosphoribosyltransferase in complex with a transition-state analogue inhibitor. *Biochemistry* **1999,** *38* (31), 9872-9880.

25. Shi, W.; Li, C. M.; Tyler, P. C.; Furneaux, R. H.; Grubmeyer, C.; Schramm, V. L.; Almo, S. C., The 2.0 Å structure of human hypoxanthine-guanine phosphoribosyltransferase in complex with a transition-state analog inhibitor. *Nat. Struct. Biol.* **1999,** *6* (6), 588-593.

26. Hazleton, K. Z.; Ho, M. C.; Cassera, M. B.; Clinch, K.; Crump, D. R.; Rosario, I., Jr.; Merino, E. F.; Almo, S. C.; Tyler, P. C.; Schramm, V. L., Acyclic immucillin phosphonates: Second generation inhibitors of *Plasmodium falciparum* hypoxanthine-guanine-xanthine phosphoribosyltransferase. *Chem. Biol.* **2012,** *19* (6), 721-730.

27. Meola, M.; Yamen, B.; Weaver, K.; Sandwick, R. K., The catalytic effect of Mg^{2+} and imidazole on the decomposition of 5-phosphoribosyl-alpha-1-pyrophosphate in aqueous solution. *J. Inorg. Biochem.* **2003,** *93* (3-4), 235-242.

28. Kaiser, M. M.; Baszczynski, O.; Hockova, D.; Postova-Slavetinska, L.; Dracinsky, M.; Keough, D. T.; Guddat, L. W.; Janeba, Z., Acyclic Nucleoside Phosphonates Containing 9-Deazahypoxanthine and a Five-Membered Heterocycle as Selective Inhibitors of Plasmodial 6-Oxopurine Phosphoribosyltransferases. *ChemMedChem* **2017,** *12* (14), 1133-1141.

29. Xu, Y.; Grubmeyer, C., Catalysis in human hypoxanthine-guanine phosphoribosyltransferase: Asp 137 acts as a general acid/base. *Biochemistry* **1998,** *37* (12), 4114-4124.

30. Eng, W. S.; Keough, D. T.; Hockova, D.; Winzor, D. J.; Guddat, L. W., Oligomeric state of hypoxanthine-guanine phosphoribosyltransferase from *Mycobacterium tuberculosis*. *Biochimie* **2017,** *135*, 6-14.

31. Guddat, L. W.; Vos, S.; Martin, J. L.; Keough, D. T.; de Jersey, J., Crystal structures of free, IMP-, and GMP-bound *Escherichia coli* hypoxanthine phosphoribosyltransferase. *Prot. Sci.* **2002,** *11* (7), 1626-1638.

32. De Clercq, E., The acyclic nucleoside phosphonates (ANPs): Antonin Holy's legacy. *Med. Res. Rev.* **2013,** *33* (6), 1278-1303.

33. Wiemer, A. J.; Wiemer, D. F., Prodrugs of phosphonates and phosphates: crossing the membrane barrier. *Topics in current chemistry* **2015,** *360*, 115-60.

34. Fattorini, L.; Piccaro, G.; Mustazzolu, A.; Giannoni, F., Targeting dormant bacilli to fight tuberculosis. *Mediterr. J. Hematol. Infect. Dis.* **2013,** *5* (1), e2013072.

35. Barry, C. E., 3rd; Boshoff, H. I.; Dartois, V.; Dick, T.; Ehrt, S.; Flynn, J.; Schnappinger, D.; Wilkinson, R. J.; Young, D., The spectrum of latent tuberculosis: rethinking the biology and intervention strategies. *Nat. Rev. Microbiol.* **2009,** *7* (12), 845-855.

36. McPhillips, T. M.; McPhillips, S. E.; Chiu, H. J.; Cohen, A. E.; Deacon, A. M.; Ellis, P. J.; Garman, E.; Gonzalez, A.; Sauter, N. K.; Phizackerley, R. P.; Soltis, S. M.; Kuhn, P., Blu-Ice and the Distributed Control System: software for data acquisition and instrument control at macromolecular crystallography beamlines. *J. Synchrotron. Radiat.* **2002,** *9* (Pt 6), 401-406.

37. Kabsch, W., Xds. *Acta Cryst. D* **2010,** *66* (2), 125-132.

38. McCoy, A. J.; Grosse-Kunstleve, R. W.; Adams, P. D.; Winn, M. D.; Storoni, L. C.; Read, R. J., Phaser crystallographic software. *J. Appl. Crystal.* **2007,** *40*, 658-674.

39. Adams, P. D.; Afonine, P. V.; Bunkoczi, G.; Chen, V. B.; Davis, I. W.; Echols, N.; Headd, J. J.; Hung, L.-W.; Kapral, G. J.; Grosse-Kunstleve, R. W.; McCoy, A. J.; Moriarty, N. W.; Oeffner, R.; Read, R. J.; Richardson, D. C.; Richardson, J. S.; Terwilliger, T. C.; Zwart, P. H., PHENIX: a

comprehensive Python-based system for macromolecular structure solution. *Acta Cryst. D* **2010,** *66* (2), 213-221.

40. Emsley, P.; Cowtan, K., Coot: model-building tools for molecular graphics. *Acta Cryst. D* **2004,** *60* (12), 2126-2132.

41. Schuttelkopf, A. W.; van Aalten, D. M., PRODRG: a tool for high-throughput crystallography of protein-ligand complexes. *Acta Cryst. D* **2004,** *60* (8), 1355-1363.

42. West, N. P.; Cergol, K. M.; Xue, M.; Randall, E. J.; Britton, W. J.; Payne, R. J., Inhibitors of an essential mycobacterial cell wall lipase (Rv3802c) as tuberculosis drug leads. *Chem. Commun. (Camb)* **2011,** *47* (18), 5166-5168.

43. Taneja, N. K.; Tyagi, J. S., Resazurin reduction assays for screening of anti-tubercular compounds against dormant and actively growing *Mycobacterium tuberculosis*, *Mycobacterium bovis BCG* and *Mycobacterium smegmatis*. *J. Antimicrob. Chemother.* **2007,** *60* (2), 288-293.

Highlights

- A new class of potent inhibitors of *Mt*HGPRT, the pyrrolidine nucleoside phosphonates and bisphosphonates, have been discovered
- Crystal structures of the *Mt*HGPRT.I complexes show how these compounds bind to the active site.
- A prodrug of these inhibitors arrest the growth of replicating and dormant TB cells